

# Impact of Athabasca oil sands operations on mercury levels in air and deposition

Ashu Dastoor<sup>1</sup>, Andrei Ryjkov<sup>1</sup>, Gregor Kos<sup>2</sup>, Junhua Zhang<sup>3</sup>, Jane Kirk<sup>4</sup>, Matthew Parsons<sup>5</sup> and Alexandra Steffen<sup>3</sup>

<sup>1</sup>Air Quality Research Division, Environment and Climate Change Canada, 2121 Trans-Canada Highway, Dorval, Québec, Canada

<sup>2</sup>Department of Chemistry and Biochemistry, Concordia University, 7141 Sherbrooke Street West, Montreal, Québec, Canada

<sup>3</sup>Air Quality Research Division, Environment and Climate Change Canada, 4905 Dufferin Street, Toronto, Ontario, Canada

<sup>4</sup>Aquatic Contaminants Research Division, Environment and Climate Change Canada, 867 Lakeshore Road, Burlington, Ontario, Canada

<sup>5</sup> Meteorological Service of Canada, Environment and Climate Change Canada, 9250 49 Street NW, Edmonton, Alberta, Canada

**Correspondence:** Ashu Dastoor (ashu.dastoor@canada.ca)

## Abstract

Oil sands upgrading facilities in the Athabasca Oil Sands Region (AOSR) in Alberta, Canada, have been reporting mercury (Hg) emissions to public government databases (National Pollutant Release Inventory (NPRI)) since the year 2000, yet the relative contribution of these emissions to ambient Hg deposition remains unknown. ~~A 3D process-based global Hg model, GEM-MACH-Hg, was applied to simulate the Hg burden in and around the AOSR using NPRI reported oil sands Hg emissions from 2012 (59 kg) to 2015 (25 kg) and other regional and global Hg emissions.~~ The impact of oil sands emissions (OSE) on Hg levels in and around the AOSR, relative to contributions from ~~sources such as~~ global (anthropogenic and, geogenic and legacy) emissions and regional biomass burning emissions (BBE), was assessed using a 3D process-based global Hg model, GEM-MACH-Hg, from 2012 to 2015. In addition, the relative importance of year-to-year changes in Hg emissions from the above sources and meteorological conditions to inter-annual variations in Hg deposition was examined. ~~Model simulated surface~~ Surface air concentrations of Hg species and ~~annually accumulated~~ annual snowpack Hg ~~in snowpacks~~ loadings simulated by the

32 model were found comparable to ~~independently obtained measurements~~ measured levels in the  
33 AOSR, suggesting consistency between reported Hg emissions from oil sands activities and Hg  
34 levels in the region. As a result of global-scale transport and long lifetime of gaseous elemental  
35 Hg (Hg(0)), surface air concentrations of Hg(0) in the AOSR reflected the background Hg(0) levels  
36 in Canada (~~1.4 ng m<sup>-3</sup>, AOSR; 1.2–1.6 ng m<sup>-3</sup>, Canada~~) with negligible impact from OSE. Highly  
37 ~~spatiotemporally variable wildfire Hg emission events led to episodes of high ambient Hg(0) air~~  
38 ~~concentrations of up to 2.5 ng m<sup>-3</sup> during the burning season.~~ By comparison, average air  
39 concentrations of total oxidised Hg (~~gaseous plus particulate~~; efficiently deposited Hg species) in  
40 the AOSR were elevated by up to 60% above background levels (2012–2013) within 50 km of the  
41 oil sands ~~major upgraders as a result of OSE.~~ Annual average Hg emission sources. Hg emissions  
42 from wildfire events led to episodes of high ambient Hg(0) concentrations and deposition  
43 enrichments in northern Alberta, including the AOSR, during the burning season. Hg deposition  
44 fluxes in the AOSR were within the range of the deposition fluxes measured for the entire province  
45 of Alberta (~~15.6–18.3 µg m<sup>-2</sup>y<sup>-1</sup>, AOSR (2012–2015); 14–25 µg m<sup>-2</sup>y<sup>-1</sup>, Alberta (2015)).~~ ~~Winter~~  
46 ~~(November–April) and summer (June–August), respectively, accounted for 20% and 50% of the~~  
47 ~~annual Hg deposition in the AOSR.~~ On a broad spatial scale, contribution from imported Hg from  
48 global sources dominated the annual background Hg deposition in the AOSR, with present-day  
49 global anthropogenic emissions contributing to 40% (< 1% from Canada excluding OSE), and  
50 geogenic ~~emissions~~ and ~~re-emissions of legacy mercury deposition~~ emissions contributing to 60%  
51 of the background Hg deposition. ~~Further, wildfire events contributed to regional Hg deposition~~  
52 ~~with enhancements of 1–13% across 200 km range of major oil sands sources.~~ In contrast, oil sands  
53 Hg emissions were responsible for significant ~~Hg deposition~~ enhancements in Hg deposition in  
54 the immediate vicinity of oil sands Hg emission sources, ~~up to 100 km in winter and up to 30 km~~  
55 ~~in summer. Hg deposition enhancements related to oil sands emissions which~~ were about ~10 times  
56 larger in winter than summer (~~average enhancement of 250–350% in winter and ~35% in summer~~  
57 within 10 km of OSE, 2012–2013). The spatial extent of the influence of oil sands emissions on  
58 Hg deposition was also greater in winter relative to summer (~100 km vs 30 km from Hg emitting  
59 facilities). In addition, ~~snowpack Hg loadings and wintertime Hg deposition displayed~~ inter-annual  
60 changes in meteorological conditions and oil sands emissions also led to significantly higher inter-  
61 annual variations in wintertime Hg deposition compared to ~~summertime deposition due to changes~~  
62 ~~in meteorological conditions (such as precipitation amounts, wind speed, surface air temperature,~~

63 ~~solar insolation, and snowpack dynamics) as well as oil sands emissions-summer.~~ For example, a  
64 large snowmelt event at the end of February in 2015 effectively removed about half of the  
65 accumulated mercury in snow, contributing to (observed and modeled) low annual snow Hg  
66 loadings. Inter-annual variations in meteorological conditions were found to both exacerbate and  
67 diminish the impacts of OSE on Hg deposition in the AOSR, which can confound the interpretation  
68 of trends in short-term environmental Hg monitoring data. In winter, within 10 km of major oil  
69 sands sources, variations in meteorology led to Hg deposition reduction by 17% in 2014 and  
70 increase by 10% in 2015 and decline in OSE lowered Hg deposition by 35% (2014) and 56% (  
71 2015), resulting in overall reductions in wintertime Hg deposition of 52% (2014) and 46% (2015),  
72 relative to 2012. By comparison, annually, changes in meteorology and BBE in 2014-2015  
73 (relative to 2012) led to Hg deposition increases of 1-6% and 2%, respectively, and decline in OSE  
74 lowered deposition by 15-22%, resulting in overall reduction in Hg deposition of 7-20% within 10  
75 km of oil sands sources. Hg runoff in spring flood, comprising the majority of annual Hg runoff,  
76 is mainly derived from seasonal snowpack Hg loadings and mobilization of Hg deposited in  
77 surface soils, both of which are sensitive to Hg emissions from oil sands developments in  
78 proximity of sources. Model results suggest that sustained efforts to reduce anthropogenic Hg  
79 emissions from both global and oil sands sources are required to reduce Hg deposition in the  
80 AOSR.

81

## 82 **Introduction**

83 Mercury (Hg) is a toxic element that accumulates in fish and mammals near the top of the food  
84 web, including humans (e.g., through consumption of contaminated fish), where it exhibits long-  
85 term toxic effects (UNEP, 2018). Hg is emitted to the atmosphere from geogenic sources such as  
86 volcanoes and the weathering of Hg-containing rocks, anthropogenic sources such as fossil fuel  
87 burning, metal smelting and artisanal gold mining, and through the re-emission of Hg historically  
88 deposited from anthropogenic and natural sources onto soils, surface waters, and vegetation  
89 (UNEP, 2013). Atmospheric Hg exists mainly in three forms: gaseous elemental mercury (Hg(0)  
90 or GEM), gaseous oxidized mercury (gaseous Hg(II); GOM), and particle bound mercury (particle  
91 bound Hg(II); PBM). The sum of GOM and PBM is referred to as total oxidised mercury (TOM)  
92 and the sum of gaseous mercury species (i.e., GEM and GOM) is referred to as total gaseous  
93 mercury (TGM) in this study. GEM/TGM and TOM are better indicators to compare observation

94 and model estimates of mercury for the purpose of this study, because of speciation uncertainties  
95 associated with the determination of GOM and PBM species (Gustin et al., 2013). Deposition of  
96 atmospheric Hg species by rain and snow (i.e., wet deposition), and by interfacial uptake on  
97 various surfaces such as soils, vegetation, water, and snowpack (i.e., dry deposition) are the  
98 pathways that contribute to Hg loadings in ecosystems. Typically, atmospheric GEM  
99 concentrations are found to be 2-3 orders of magnitude higher (in the low ng m<sup>-3</sup> range) than GOM  
100 and PBM (typically in the lower pg m<sup>-3</sup> range) because GEM is the dominant atmospheric Hg  
101 species emitted to air and the reactivity of the latter (GOM and PBM) leads to efficient dry and  
102 wet deposition removal of these species close to sources. Stability and volatility of GEM results  
103 in its long lifetime in the atmosphere, with six months to one year, allowing for transport and  
104 distribution on a global scale, and re-emission from planetary surfaces (UNEP, 2013).

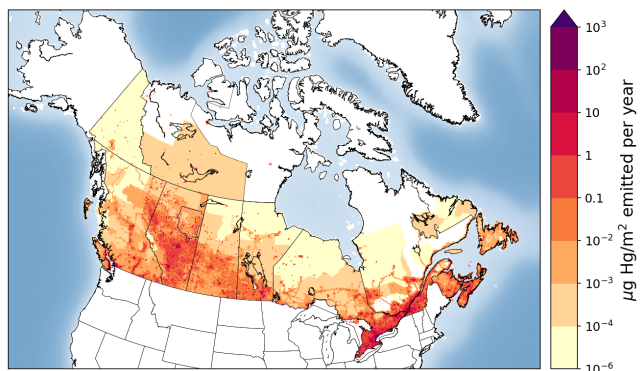
105  
106 On a global scale, dry deposition of GEM by vegetation-uptake over land and wet deposition of  
107 TOM produced by atmospheric oxidation of GEM are the dominant pathways of Hg removal  
108 (Obrist et al. 2016; Wright et al., 2016; Zhou et al. 2021). Primary emissions of GOM and PBM  
109 from industrial sources are an important contributor to dry and wet depositions of Hg on a local to  
110 regional scale. Once Hg is deposited to surfaces, it can be reduced and re-emitted back as GEM to  
111 the air and, thus, Hg redistributes and accumulates in the aquatic and terrestrial environments  
112 globally. Hg also inhibits enzymatic processes and reacts with organic compounds. This leads to  
113 the formation of toxic, and bioaccumulating, methyl-Hg, primarily in aquatic systems, which is  
114 the principal cause of a severe neurological syndrome known as “Minamata Disease”. In order to  
115 reduce the amount of Hg released to the environment and limit its exposure to humans, an  
116 international treaty, the Minamata Convention on Mercury, was adopted in 2017 (UN, 2017).

117  
118 Anthropogenic emissions of Hg to air from global sources stand at an estimated 2220 t y<sup>-1</sup> in 2015  
119 (UNEP, 2018). Canadian anthropogenic Hg emissions were estimated at about 4.3 t y<sup>-1</sup> (less than  
120 0.2% of global anthropogenic emissions) in 2015, with an estimated 58% coming from point  
121 sources such as coal-fired power plants and smelters, and 42% from area sources (Zhang et al.,  
122 2018; see Figure 1). Anthropogenic Hg emissions in Canada have declined by 85% from 1990 to  
123 2010 (from ~35 to 5 t y<sup>-1</sup>), with major reductions from sectors such as the non-ferrous metal  
124 mining and smelting (-98%), chemical industries (-95%), waste (-76%), iron and steel industries

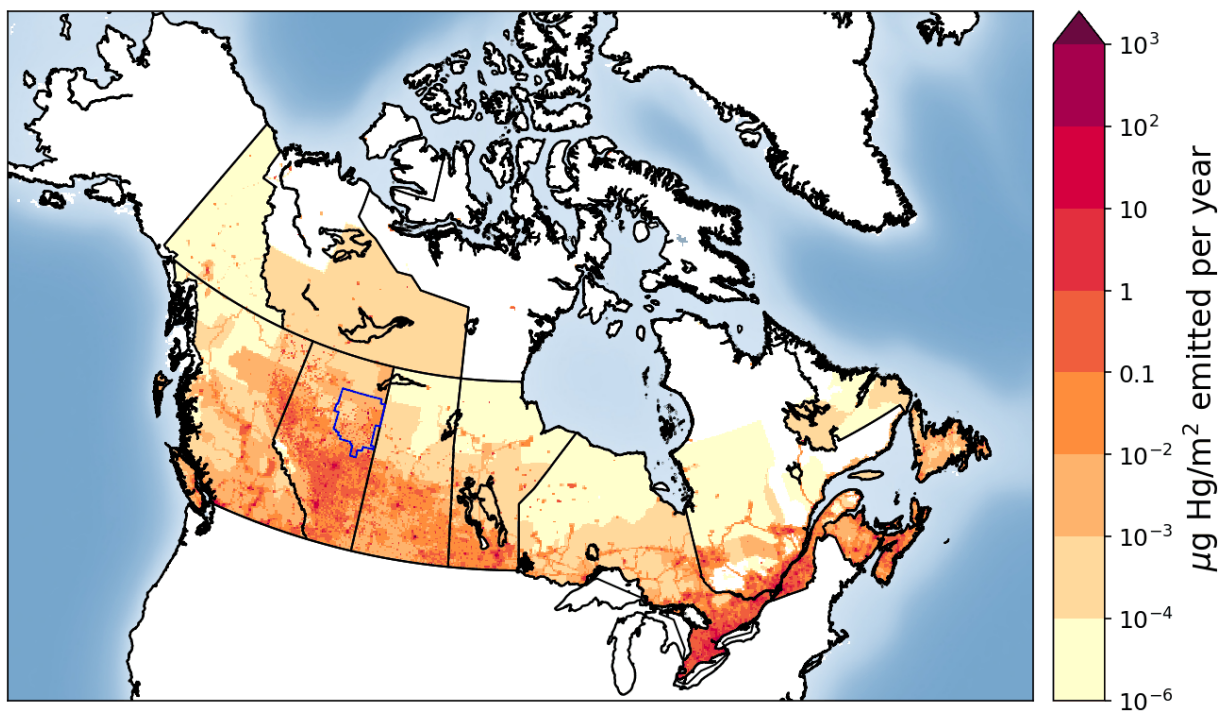


125 (-54%) and electric power generation (-30%) (CMSA, 2016). However, due to the steady increase  
126 in development of the oil sands, the upstream petroleum sector has shown increases in Hg  
127 emissions and accounted for approximately 4.6% of the total Canadian Hg emissions in 2010  
128 (CMSA, 2016).

129



130

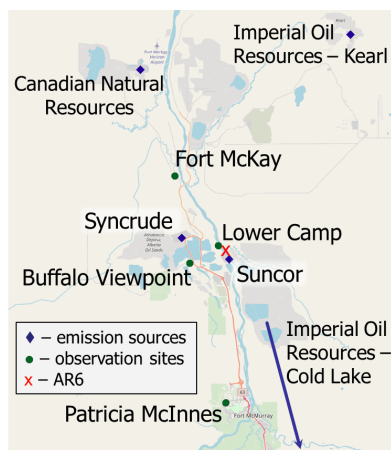


131 Figure 1: Spatial distribution of anthropogenic Hg emissions in Canada in 2015 (~ 4.3 t/y). The  
132 Athabasca Oil Sands Region is indicated with an approximate rectangular blue shape within  
133 northeastern Alberta, bordering Saskatchewan.

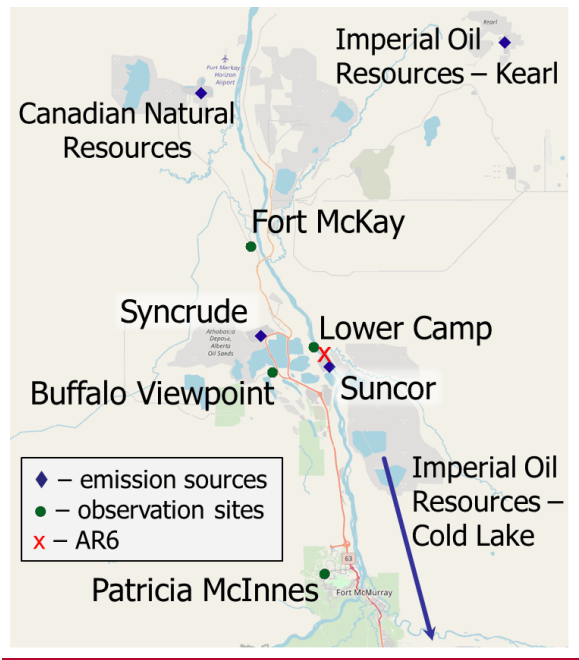
134

135 The Athabasca Oil Sands Region (AOSR) in the northeastern portion of the Canadian province of  
136 Alberta (see Figure 1) is a zone of extensive natural resource development. The large natural

137 deposits of bitumen, a heavy crude oil, contained in a mixture of water and clay (called “oil sands”)  
138 has led to establishment of large-scale mining and upgrading activities in the area north of Fort  
139 McMurray, Alberta (AB) (see map Figure 2). Surface mining and in-situ recovery methods are  
140 used to extract bitumen and then upgrade it to synthetic crude oil (Alexander and Chambers, 2016;  
141 Larter and Head, 2014). Point source emissions of organics and heavy metals, including Hg,  
142 originate from mining activities and upgrading facilities in the AOSR. The upgraders are operated  
143 by the companies Suncor, Syncrude, and Canadian Natural Resources. The upgrading process also  
144 includes the removal of impurities consisting of sulfur and nitrogen-containing compounds by  
145 catalytic hydrotreatment, with volatile hydrogen sulfide and ammonia as by-products. Trace metals  
146 contained in the heavy asphaltene fraction are also removed by either stabilization, rejection, or  
147 upgrading of asphaltenes (Jia, 2014). The yearly amounts of total Hg emissions from Athabasca  
148 oil sands facilities, for the years 2012 to 2015, were between 69 and 25 kg. These annual emissions  
149 exhibited an overall downward trend (for details see Table 1 and Figure 3).



150



151

152 Figure 2: Map of the AOSR with the main point sources for Hg emissions from oil sands  
 153 developments, and air observation sites. “AR6” marks the approximate midpoint of operations as  
 154 defined by Kelly et al. (Kelly et al., 2010).

155

156 In 2010, Kelly et al., reported increased concentrations of 13 different trace metals including Hg  
 157 in the surface waters of the Athabasca River and its tributaries in the oil sands region (Kelly et al.,  
 158 2010). Observed concentrations were higher near oil sands operations than away from the potential  
 159 sources. Comparison of upstream and downstream data showed consistently higher concentrations  
 160 for downstream sites. A similar set of observations was made for Hg in surface snow samples,  
 161 more specifically, Hg bound to particulates. Concentrations in accumulated snow collected near  
 162 oil sands developments in March averaged 861 ng m<sup>-2</sup> compared to less than 100 ng m<sup>-2</sup> for  
 163 background measurements (Kelly et al., 2010). Several oil sands installations were identified as  
 164 potential sources for the elevated observations of Hg, but no direct link between sources and  
 165 observations was established. Specifically, upgraders were discussed as a source for high Hg levels  
 166 in the region. Other potential sources included fly ash, road dust, land clearing and mining  
 167 operations.

168

169 To address the lack of Hg monitoring and attribution of sources, as concluded by Kelly et al.  
 170 (2010), several follow-up studies were conducted with the intention to establish a conclusive link

171 between measured pollutant concentrations and potential sources in the AOSR (Kelly et al., 2010;  
172 Cooke et al., 2017; Kirk et al., 2014; Emmerton et al., 2018; Lynam et al., 2018; Willis et al., 2019;  
173 Willis et al., 2018; Gopalapillai et al., 2019). In addition to water and snow samples, other media  
174 have been investigated, such as air, biota and sediments. Cooke et al. (2017) studied lake sediment  
175 cores sampled from 20 lakes at various distances from oil sands operations, including two of them  
176 in the near vicinity (i.e., within 20 km) of the two major upgrading facilities (Suncor and Syncrude)  
177 within the region (or site AR6 as designated by Kelly (2010)) (Cooke et al., 2017). The cores  
178 provided trace metal data for approximately the past 100-250 years. The cores showed that Hg  
179 concentrations have increased by a factor of 3, reflecting the generally accepted scientific finding  
180 that global Hg has increased 3-fold as a result of anthropogenic activities since the industrial  
181 revolution. No additional increase of Hg concentrations was detected related to the beginning of  
182 oil sands operations in the late 1960s. This contrasts with Kelly et al. (2010) and the follow-up  
183 study by Kirk et al. (2014) that showed higher Hg loadings in the accumulated snowpack and  
184 surface water sampled closer to the mining and upgrading facilities in the AOSR in early spring  
185 (March), mostly consisting of PBM of atmospheric origin. While Hg levels were closely correlated  
186 with other trace metal concentrations originating from oil sands activities such as nickel and  
187 vanadium, no direct causal link with air emissions of Hg, as reported to the National Pollutant  
188 Release Inventory (NPRI), was established. Gopalapillai and coworkers recently reported temporal  
189 trends in snowpack loadings of total Hg (THg) and methyl mercury (MeHg) (and 44 other  
190 elements) (Gopalapillai et al., 2019). Using a composite of snowpack profile samples collected  
191 between 2011 and 2016 and data from previous campaigns, a decrease in THg loadings from an  
192 average of 510 ng m<sup>-3</sup> in 2008 to 175 ng m<sup>-3</sup> in 2016 was found within 8 km from AR6. However,  
193 due to the limited temporal coverage (with measurements for THg starting in 2008), the authors  
194 suggested a need for additional studies to understand the impact of Hg in the AOSR.

195  
196 A recent study by Emmerton et al. (2018) examined lake water samples and related observed Hg  
197 and methyl-Hg concentrations to local geology, watershed conditions, and to oil sands activities,  
198 with the latter only contributing an estimated <2% of the overall Hg deposited (Emmerton et al.,  
199 2018). Long-range transport and biomass burning (i.e., forest fires) were suggested to be the major  
200 sources of Hg (Emmerton et al., 2018). Similarly, in a recent study of wet deposition data by  
201 Lynam et al. (2018), very low fluxes of Hg deposition were calculated, though the study sites used

202 (AMS6, the Patricia McInnes observation site shown in Fig. 1) were located further away from  
203 emitters. Results suggested that dry deposition could, instead, be a more important pathway of Hg  
204 removal in the region (Lynam et al., 2018).

205  
206 In an effort to explain the elevated Hg concentrations found in the snowpack and waters near oil  
207 sands mining and upgrading activities, tailings ponds were studied as a potential source of Hg  
208 emissions related to oil sands activities (Willis et al., 2018). However, the water in these ponds  
209 (i.e., the non-recycled portion of process water used to process mined bitumen) were found to be  
210 an insignificant source of THg and MeHg.

211  
212 The above-mentioned studies illustrate recent progress in the ongoing effort to examine the link  
213 between observed concentrations and anthropogenic sources of Hg in the AOSR. However, in  
214 addition to local emissions, multiple other sources of mercury emissions impact the region,  
215 especially forest fires and worldwide anthropogenic and geogenic (contemporary and legacy)  
216 emissions that are atmospherically transported into the region. Owing to the much larger emissions  
217 of Hg from worldwide sources, as compared to Canadian sources, and the long lifetime of Hg in  
218 air, imported Hg accounts for the majority of the Hg burden in Canada (CMSA, 2016), rendering  
219 the assessment of the impacts of domestic Hg emissions challenging using measurements alone.  
220 While Cooke et al. (2017) investigated the history of Hg deposition in lake catchments via the  
221 study of sediment cores, only two lakes sampled were close enough (within 20 km) to oil sands  
222 activities, whereas most sites were 20 to >50 km away from the oil sands facilities.

223  
224 After Hg is emitted to air from oil sands mining and upgrading activities, transport, transformation  
225 and deposition processes determine the distribution and amounts of Hg deposited to environmental  
226 media such as vegetation, soils, and water bodies. 3D process-based predictive atmospheric  
227 composition models include process representations (such as atmospheric transport, chemical  
228 transformations, aerosol particle formation and growth, and wet and dry deposition of gases and  
229 particles) and simulate spatiotemporal distributions of pollutants in air and deposition starting from  
230 emissions (anthropogenic and natural) as inputs. These models provide insight into transport and  
231 transformation pathways of pollutants and causal links between emissions and concentrations  
232 observed in environmental media. Models have been applied to study Hg source attribution on

233 global and regional scales, answering questions such as how much a specific emission source  
234 contributes to local and regional air concentrations and deposition, and how does the pollutant  
235 burden change as industrial activity and related emissions vary (UNEP, 2008; CMSA, 2016;  
236 UNEP, 2018)? Model processes are typically constrained by evaluating simulated pollutant levels  
237 using observation data from ground-based monitoring networks and research campaigns.  
238 Additionally, aircraft measurement data provide observation data on the vertical scale.

239  
240 Wildfires are important sources of Hg in Northwestern Canada and climate change is intensifying  
241 their frequency (Fraser et al., 2018). Biomass burning primarily releases legacy Hg previously  
242 deposited to foliage and soils (Friedli et al., 2001; De Simone et al., 2015). Using multivariate data  
243 analysis, Parsons et al. (2013) determined contribution from local sources (i.e., oil sands activities)  
244 to be minimal as compared to total gaseous Hg concentrations in the air in the AOSR; however,  
245 the authors noted significant episodes of regional forest fires impacting the observed Hg  
246 concentrations in the air during the summer months (Parsons et al., 2013).

## 247 248 **Objectives**

249 Observations of atmospheric Hg in the AOSR are limited to surface air GEM concentrations and  
250 Hg loadings in snow. Summertime wet and dry deposition is not measured. Therefore, measured  
251 estimates of annual Hg deposition in AOSR is currently not possible. Furthermore, a quantification  
252 of the relative importance of different Hg emission sources responsible for Hg loadings in the  
253 AOSR is required to prioritize mitigation actions. The 3D mercury model, Global Environmental  
254 Multiscale - Modelling Air quality and CHemistry – Mercury (GEM-MACH-Hg), was applied to  
255 develop a comprehensive understanding of atmospheric Hg and deposition levels and pathways,  
256 and the role of emissions from Athabasca oil sands activities (particularly from bitumen upgraders)  
257 on the spatiotemporal distribution of Hg deposition in AOSR. This study addresses the following  
258 questions:

- 259 1. How do air concentrations and ecosystem loadings of Hg species in AOSR compare to  
260 other regions in Canada?
- 261 2. What is the level and geographical extent of the contribution of Athabasca oil sands  
262 emissions on Hg in air and deposition?

263 3. How does the impact of oil sands development on Hg levels in the region compare with  
264 the impacts of two other major sources of Hg in the region, biomass burning and global  
265 emissions?

266 4. What controls the inter-annual variability in Hg levels in AOSR?  
267

268 This is the first study that provides a direct connection between Athabasca oil sands Hg emissions  
269 and deposition of Hg in and around the AOSR. A similar approach using the model GEM-MACH-  
270 Hg was previously applied to the assessment of Hg source apportionment at national and global  
271 scales (CMSA, 2016; AMAP/UNEP, 2013; UNEP, 2018).  
272

### 273 **The model and emission inputs**

274 GEM-MACH-Hg (Dastoor et al., 2015) is the mercury version of Environment and Climate  
275 Change Canada's 3D process-based operational air quality forecast model GEM-MACH (Global  
276 Environmental Multiscale - Modelling Air quality and Chemistry; Makar et al., 2018; Whaley et  
277 al., 2018). GEM-MACH includes emissions of gases and aerosols, and simulates meteorological  
278 processes, aerosol microphysics, tropospheric chemistry and pollutant dry and wet removal  
279 processes from the atmosphere. In addition, GEM-MACH-Hg includes emissions, chemistry and  
280 dry and wet removal processes of three Hg species (GEM, GOM and PBM) (Dastoor and Durnford  
281 2014; Dastoor et al., 2008; Durnford et al., 2012; Fraser et al., 2018; Kos et al., 2013; Zhou et al.  
282 2021). The recent version of GEM-MACH-Hg, previously applied to the investigation of the  
283 importance of biomass burning emissions to the Hg burden in Canada (Fraser et al., 2018) and the  
284 role of vegetation Hg uptake (Zhou et al. 2021), was used in this study. Oxidation of GEM and  
285 gas-particle partitioning of oxidized Hg species (GOM and PBM) are the main chemical  
286 transformation processes, and dry deposition of GEM, GOM and PBM, and wet deposition of  
287 GOM and PBM are the major removal pathways of Hg in the model. Since observations of  
288 snowpack Hg loadings at the end of the winter season are utilized for model evaluation in this  
289 study, a detailed representation of the air-cryosphere Hg exchange and transformation processes  
290 is important. GEM-MACH-Hg includes a dynamic multilayer air-snowpack-meltwater Hg  
291 parameterization, representing Hg accumulation by precipitation and dry deposition to snowpacks,  
292 vertical diffusion and redox reactions in snowpacks, and re-volatilization and meltwater run-off of  
293 Hg species (Durnford et al., 2012). Geospatially distributed global, regional and local emissions



294 of Hg species (GEM, GOM and PBM) to air from primary geogenic and anthropogenic sources  
295 and re-emissions of previously deposited Hg (legacy Hg) from terrestrial and oceanic surfaces are  
296 included in the model.

297  
298 Three geographical domains were utilized for the model simulations in this study: global, North  
299 America (NA) and AOSR. A geospatial resolution of 10 km was chosen for the NA domain and  
300 its boundary conditions were determined by the global simulations conducted at  $1^0 \times 1^0$  latitude-  
301 longitude resolution. Model simulations for the AOSR were carried out at a finer geospatial  
302 resolution of 2.5 km for an extended AOSR domain with the approximate midpoint adjacent to the  
303 two largest upgrading facilities (called “AR6”) (Kelly et al., 2010) and extending as far north as  
304 Hay River, NT, and as far south as Red Deer, AB; the approximate western and eastern extents of  
305 the domain are marked, respectively, by Grande Prairie, AB and Flin Flon, MB.

306  
307 Geogenic emissions and re-emissions of legacy Hg in soils and oceans ( $\sim 4200 \text{ t y}^{-1}$ ) emitted as  
308 GEM were distributed as described in Durnford et al., (2012). Wildfire biomass burning Hg  
309 emissions are represented in the model simulations using the FINN (Fire INventory) fire emissions  
310 products (Wiedinmyer and Friedli, 2007; Wiedinmyer et al., 2011) together with vegetation-  
311 specific emission factors (EFs) as described in Fraser et al. (2018). FINN estimated biomass  
312 burning Hg emissions (emitted as GEM) were  $\sim 600 \text{ t y}^{-1}$  globally, and 10.8 (2012), 11.4 (2013),  
313 15.5 (2014) and 11.1 (2015) Mg/y in Canada, and 13.4 (2012), 10.5 (2013), 11.4 (2014) and 9.5  
314 (2015) Mg/y in the US.

315  
316 Contemporary global anthropogenic Hg emissions for 2015 ( $2224 \text{ t y}^{-1}$ ; subdivided into GEM,  
317 GOM and PBM) developed by the Arctic Monitoring and Assessment Programme (AMAP)  
318 (UNEP, 2018) were incorporated into the model for the global scale simulations. For NA and  
319 AOSR domains, GEM-MACH-Hg includes monthly and diurnally varying anthropogenic Hg  
320 emissions in Canada developed by Zhang et al. (2018), based on the NPRI (NPRI) database (2013)  
321 for the major point sources and the 2010 Air Pollutant Emission Inventory (APEI) for the area  
322 sources. Anthropogenic Hg emissions in the United States included in GEM-MACH-Hg were  
323 based on the 2011 National Emissions Inventory (NEI) (EPA), described in Zhang et al., (2018).  
324 Total anthropogenic emissions of Hg in Canada, the United States and worldwide were 4.3, 47 and

325 2224 t y<sup>-1</sup>, respectively. The GEM:GOM:PBM ratio in the total anthropogenic Hg emissions was  
326 approximately 70%:23%:7%.

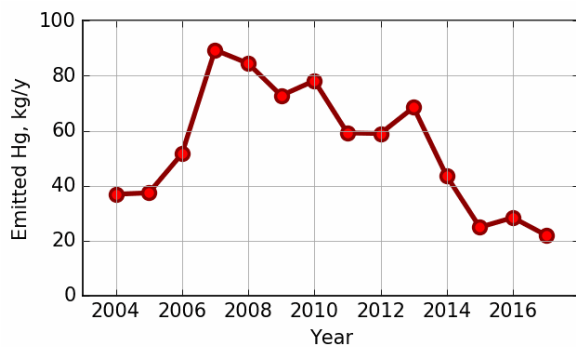
327  
328 For the oil sands activities related Hg emissions, the model's input consisted only of NPRI-  
329 reported air emissions. ~~Possibility~~Possibility of fugitive dust from the disturbed landscape due to  
330 oil sands activities as a source of particulate-bound Hg emissions was noted by Kirk et al. (2014).  
331 Cooke et al. (2017) were unable to detect Hg from dust emissions in lake sediments. Comparison  
332 of modeled and observed Hg levels conducted in this study allowed an assessment of whether  
333 NPRI reported oil sands emissions and area sources (APEI) in AOSR capture Hg emissions in the  
334 region comprehensively or whether there are other yet undetermined important sources of Hg  
335 emissions such as from fugitive dust in the AOSR.

336  
337 NPRI is a mandatory reporting tool for a wide range of contaminants, including Hg, as prescribed  
338 by the Canadian Environmental Protection Act. Facilities are required to report Hg releases, if total  
339 work hours exceed 20,000 and if a reporting threshold of 5 kg y<sup>-1</sup> is met for Hg and Hg containing  
340 compounds that were manufactured, processed or otherwise used (includes by-products) or  
341 contained in tailings and waste rock. For the AOSR domain, Hg emissions were updated in the  
342 model from 2012 to 2015 using the NPRI point source Hg emissions data for each year. A summary  
343 of Hg emissions from Athabasca oil sands upgrading facilities (NPRI) for 2012-2015 and temporal  
344 trend from 2004-2017 are available in Table 1 and Figure 3, respectively. Based on NPRI, total  
345 anthropogenic Hg emissions in Canada from the province of Alberta were 605 kg in 2015. Among  
346 these, fossil fuel burning activities such as coal-fired power plants, waste incineration facilities  
347 and other fossil fuel combustion contributed an estimated 221, 120 and 72 kg, respectively, which  
348 represents 68% and, therefore, the bulk of total anthropogenic Hg emissions in Alberta. Iron and  
349 steel production together with the cement industry (emitting 55 and 46 kg, respectively) contribute  
350 another 14% and oil sands upgrading was a minor contributor (~ 25 kg) in 2015.

351

Facility	Latitude	Longitude	2012	2013	2014	2015
Suncor Energy	57.0033	111.466	35	37	0.439	-
Syncrude - Mildred Lake	57.0405	111.619	17	23	30	9.9
Imperial Oil Resources - Cold Lake	54.597	110.399	7	7.4	8.8	11
Imperial Oil Resources - Kearl	57.3969	111.071	-	1.1	4.3	4
<b>Sum of all four sources</b>			<b>59.0</b>	<b>68.5</b>	<b>43.5</b>	<b>24.9</b>

352 Table 1: Athabasca Oil Sands Hg emissions (all in kg<sub>yr<sup>-1</sup></sub>) reported to NPRI by oil sands  
353 processing facilities, and used in the model. For the location of facilities in the AOSR see Figure  
354 2.



356

357

358 Figure 3: Time series of total Hg emissions from oil sands processing facilities in the AOSR. Data  
359 was compiled from the NPRI database. Numerical values and individual contributions from 2012-  
360 2017 are available in Table 1.

361

362 **Model simulations**

363 Base model simulations at the three model simulation domains (i.e., global, NA and AOSR) were  
364 performed using all sources of Hg emissions (as described earlier) and meteorological conditions  
365 for the respective years from 2010 – 2015 to allow evaluation of modeled air concentrations with  
366 measured air concentrations for all available years in the AOSR. Snowpack Hg measurements in  
367 the AOSR started in 2012. Thus, the model-measurement comparison of snowpack Hg and the oil  
368 sands Hg emissions impact study was conducted for the years 2012-2015.

369  
370 Multiple controlled model simulations from 2012-2015 were performed choosing appropriate  
371 geographic domains to assess the relative role of Athabasca oil sands Hg emissions on Hg burden  
372 in the AOSR. The impact of Athabasca oil sands emissions was assessed by zeroing out emissions  
373 of Hg from oil sands facilities in a controlled simulation using the AOSR domain. Contributions  
374 of Hg emissions from biomass burning (in North America) and global anthropogenic sources to  
375 the AOSR Hg levels were obtained by zeroing out emissions from these sources in controlled  
376 simulations on North America and global model domains, respectively. Source apportionment of  
377 the anthropogenic Hg deposition from worldwide sources was conducted using a series of global-  
378 scale controlled simulations by zeroing out anthropogenic Hg emissions in different source  
379 regions. In addition, controlled model simulations were performed to estimate the individual  
380 influences of meteorology, biomass burning emissions and oil sands emissions on the interannual  
381 variations in Hg deposition in the AOSR by successively adding these three temporal changes in  
382 2013-2015.

383  
384 **Mercury observations in the AOSR**

385 Simulated air concentrations and deposition of Hg were evaluated with observations of Hg in air  
386 and snowpack in the AOSR. These measurements were recorded with instruments deployed for  
387 air quality monitoring purposes and to study the atmospheric deposition of Hg species in the AOSR  
388 (Parsons et al., 2013; Kirk et al. 2014; Gopalapillai et al., 2019). Air measurements were carried  
389 out at three sites in the AOSR: Patricia-McInnes (2010-2018), Fort Mackay (2014-2018), and  
390 Lower Camp (2012-2014). Measurements were made using Tekran 2537 Hg analysers for GEM,  
391 and Tekran 1130/1135/2537 systems for speciated Hg (GOM and PBM) fitted with PM<sub>2.5</sub> and  
392 PM<sub>10</sub> inlets (see map in Figure 2 for equipment placement and Figure 4-6 for data). Standard

393 operating procedures were provided by the Canadian Atmospheric Mercury Measurement  
394 Network (CAMNet, (Steffen and Schroeder, 1999)). Air measurements of oxidized Hg  
395 concentrations were carried out at only one site near Fort McKay in 2015 (Parsons et al., 2013).  
396 Since Hg deposition to snow is mainly derived from the ambient oxidized Hg concentrations,  
397 observations of snowpack Hg loadings provide additional constraint for modeled oxidized Hg  
398 concentrations in air.

399  
400 Snow samples were collected from 2012 to 2015 at 454 sites located at varying distances from the  
401 major upgrading facilities (<1-231 km) to estimate total seasonal Hg loadings in surface snow in  
402 the AOSR (Gopalapillai et al., 2019; Kirk et al., 2014). Specifically, 90 (2012), 86 (2013), 140  
403 (2014) and 138 (2015) samples were obtained from sites located close to the AOSR emission  
404 sources (< 25 km) and at background sites further away from sources (> 120 km). Sample  
405 collection was carried out in early to mid-March of each year at approximate maximum snowpack  
406 depth based on Environment and Climate Change Canada's National Climate Data and  
407 Information Archive historical snow accumulation data (GoC, 2019). Kirk et al. (2014) employed  
408 ultra-clean handling and analysis protocols while taking care to avoid local contamination from  
409 transportation since sites were accessed by helicopter and snowmobile. Mercury analysis in the  
410 snow was carried out using cold vapour atomic fluorescence spectroscopy (Willis et al., 2018; Kirk  
411 et al., 2014; EPA, 1996; Bloom and Crecelius, 1983). The determined snowpack Hg loading at the  
412 end of the winter season represents lower limit of the net wintertime dry and wet deposition of Hg.  
413 Hg deposited to snowpacks is partially reduced and re-volatilized to the air and lost during intra-  
414 seasonal snowpack melting. Summertime measurements of Hg deposition by scavenging in rain  
415 and direct uptake by vegetation, soils and waters were unavailable for model evaluation.

## 416 417 **Results and Discussion**

### 418 **Evaluation of model simulated mercury concentrations in air**

419 GEM-MACH-Hg has been extensively evaluated with comprehensive worldwide (including  
420 Canada) observations, inter-compared with other Hg models, and applied to mercury assessments  
421 in previous studies (Angot et al., 2016; Bieser et al., 2017; Dastoor et al., 2008; Dastoor and  
422 Durnford, 2014; Durnford et al., 2010; Durnford et al., 2012; Fraser et al., 2018; Kos et al., 2013;  
423 Travnikov et al., 2017; Zhou et al. 2021; AMAP 2013; CMSA, 2016; UNEP, 2018). Model

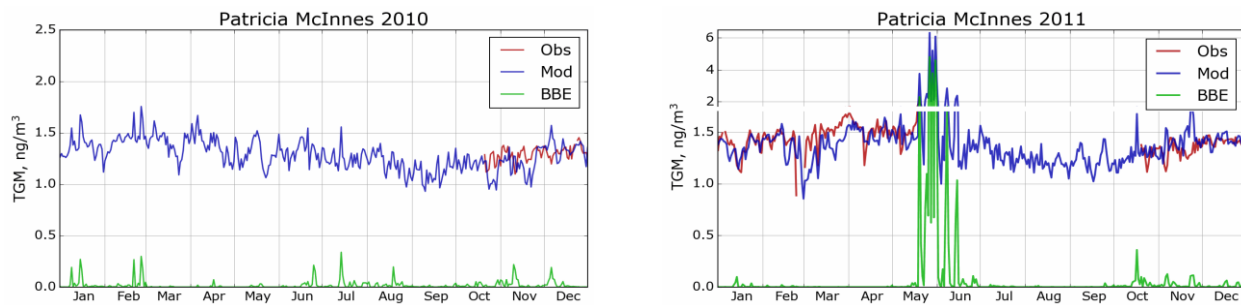
424 evaluation of ambient Hg in the AOSR is presented in this study. Figures 4-6 provide a comparison  
425 of simulated (blue trace) and observed (red trace) daily averaged TGM concentrations in air at the  
426 three observation sites (Figure 4: Patricia McInnis, 2010-2015; Figure 5: Lower Camp, 2012-2014;  
427 and Figure 6: Fort McKay, 2014-2015), and how the model captured biomass burning events  
428 (BBE) (green traces show modeled biomass burning contributions to TGM concentrations). While  
429 some observations are incomplete (e.g., June 2013, Patricia McInnis), the data provide a detailed  
430 picture of TGM surface concentrations near oil sands activities (see Figure 2 for details). In  
431 general, data from all three observation sites and model simulation results agreed well with an  
432 average squared Pearson correlation coefficient of 0.6, and measured and modeled median TGM  
433 concentrations ( $\pm$  standard deviation) of  $1.34\pm 0.21$  and  $1.39\pm 0.17$  ng m<sup>-3</sup> (2011-2015) at Patricia  
434 McInnis,  $1.36\pm 0.17$  and  $1.36\pm 0.18$  ng m<sup>-3</sup> (2013) at Lower Camp and  $1.22\pm 0.23$  and  $1.33\pm 0.19$   
435 ng m<sup>-3</sup> (2014-2015) at Fort McKay, respectively. The model captured the observed seasonal cycle  
436 (typical in the northern hemisphere) with spring maxima and fall minima, shaped mainly by  
437 surface fluxes of Hg such as the dominance of re-emission fluxes of Hg from snow in winter and  
438 spring, and uptake of Hg by vegetation in summer and fall- [\(Zhou et al. 2021\)](#). Transport of Hg  
439 from biomass burning (i.e., wildfires) events in northern and western Canada yielded distinct Hg  
440 concentration peaks in TGM concentrations in the AOSR (Figures 4-6). For 2011, biomass burning  
441 provided a large contribution to overall TGM concentrations, which peaked during these events at  
442 Patricia McInnis; however, no concurrent observations were available for the months of May and  
443 June. During the large wildfire events in 2012 and 2015 (June-July), daily averaged TGM  
444 concentrations were generally  $< 2.5$  ng m<sup>-3</sup>, which were accurately reproduced by the model.  
445 However, as shown in Figure 5 for the Lower Camp site in August 2013, there are discrepancies  
446 between modeled and observed wildfire events. The impacts of biomass burning emissions on Hg  
447 burden in Canada and the uncertainties in wildfire Hg emissions associated with the  
448 characterization of wildfire events and emission levels using satellite and field data were described  
449 in a previous study (Fraser et al., 2018). Low TGM concentration events in winter and early spring,  
450 such as those in March 2014 at Patricia McInnis, were typically associated with clean air masses  
451 coming from the Arctic in AOSR. Model-measurement agreement of TGM levels in the air is  
452 within the respective model and measurement uncertainties and indicates that reported Hg  
453 emissions from AOSR facilities are reasonable.

454

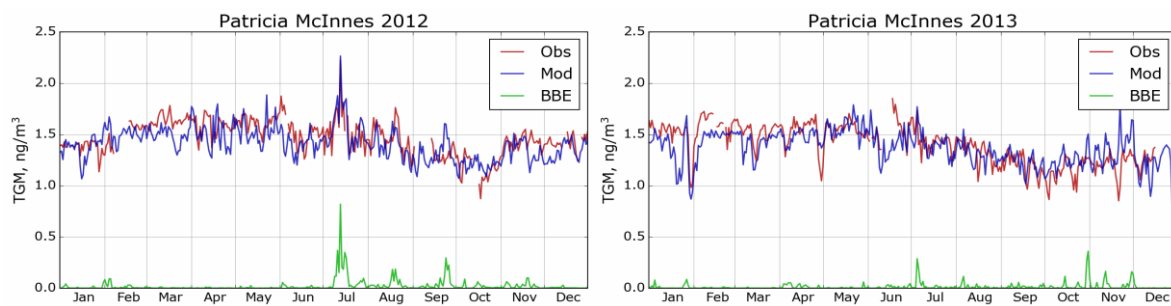
455 GOM and PBM observations were conducted at Fort McKay (a region dominated by natural boreal  
456 forest) using PM<sub>2.5</sub> (captures particle sizes < 2.5 μm) and PM<sub>10</sub> (captures particle sizes < 10.0 μm)  
457 inlets in AOSR for 2015, but significant measurement data gaps were present particularly in winter  
458 and spring. Observed annual average concentrations were 1.02 ± 2.59 (GOM) and 3.47 ± 4.79 pg  
459 m<sup>-3</sup> (PBM) using the PM<sub>2.5</sub> inlet, and 0.60 ± 1.11 (GOM) and 4.25 ± 8.23 pg m<sup>-3</sup> (PBM) using the  
460 PM<sub>10</sub> inlet in 2015; these observations suggest a dominance of PBM in fine particles (< 2.5 μm)  
461 at the Fort McKay site (17 km Northwest of AR6). The model simulated and observed average  
462 TOM air concentrations and standard deviation (± 1σ) in 2015 were 4.74 ± 5.06 pg m<sup>-3</sup> and 5.74 ±  
463 7.20 pg m<sup>-3</sup>, respectively; observed data from both inlets was combined to reduce measurement  
464 gaps. Episodes of high concentrations of particulate Hg (up to 72.9 pg m<sup>-3</sup>), occurring  
465 predominantly on coarse (> 2.5 μm) particles, that were absent in the modeled PBM  
466 concentrations were observed in March. The sources of coarse particles in the AOSR are currently  
467 unknown, but fugitive dust from pet coke piles and roads as a result of oil sands mining activities  
468 was suggested by Gopalapillai et al. 2019. It should be noted that uncertainty of a factor of 2 or  
469 higher with oxidized Hg measurements has been reported (Kos et al., 2013; Gustin et al. 2015).  
470 Comparable average GOM and PBM concentrations of 1.89 ± 8.31 and 3.82 ± 4.90 pg m<sup>-3</sup> (mean  
471 ± 1σ, 2009-2011), respectively, have been measured at a site 8 km from a coal-fired power plant  
472 in Genesee, AB (about 500 km southwest of Fort McMurray). Seasonal cycles at the two sites  
473 (Fort McKay and Genesee) were similar, with TOM maxima in May-June. Since Hg deposition to  
474 snow is primarily driven by the uptake of ambient oxidized Hg species in snowfall and snowpack,  
475 the robustness of model simulated oxidized Hg in air was further tested by comparing modeled  
476 snowpack Hg loadings with measurements (see next section).  
477



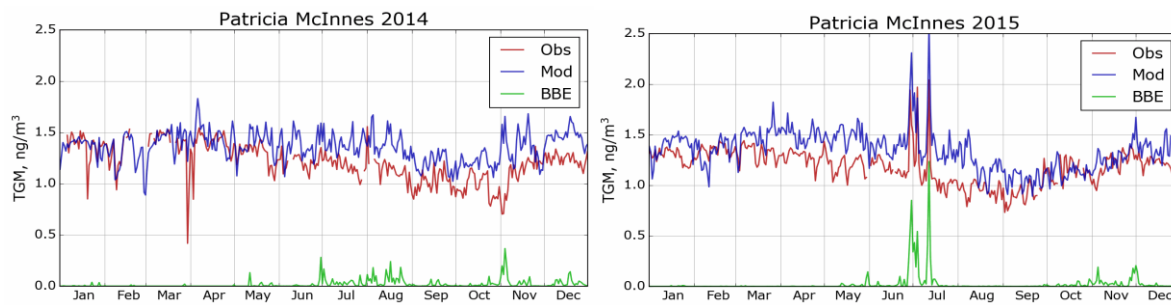
478



479



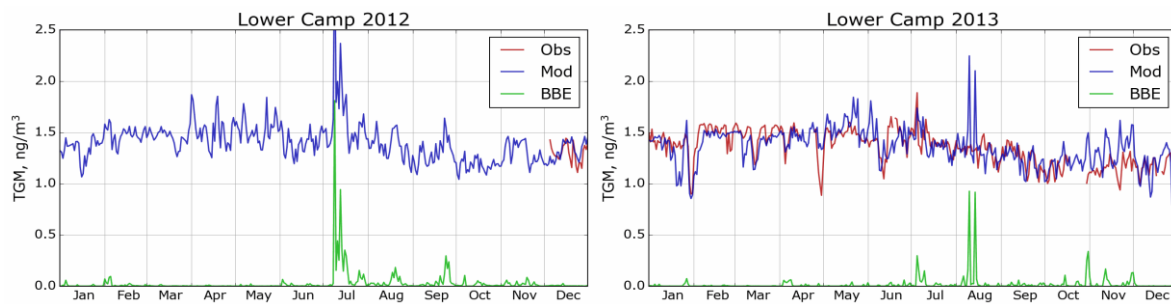
480

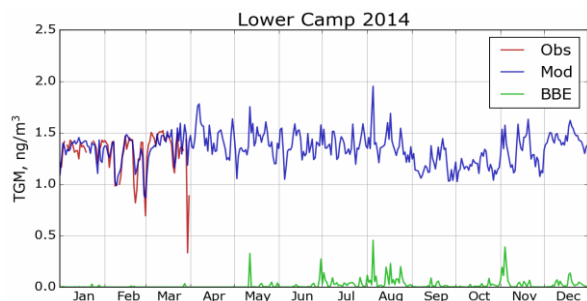


481 Figure 4: Simulated and observed daily averaged surface air TGM concentrations in AOSR for the  
 482 site Patricia-McInnes (2010—2015). Obs – observations; Mod – model estimation; BBE –  
 483 modeled biomass burning contributions. Note the larger range of the y-axis to plot the strong  
 484 biomass burning event in May and June of 2011.

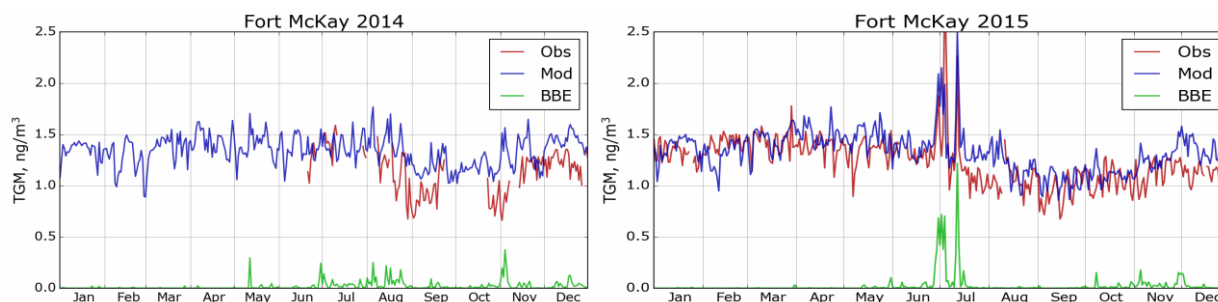
485

486





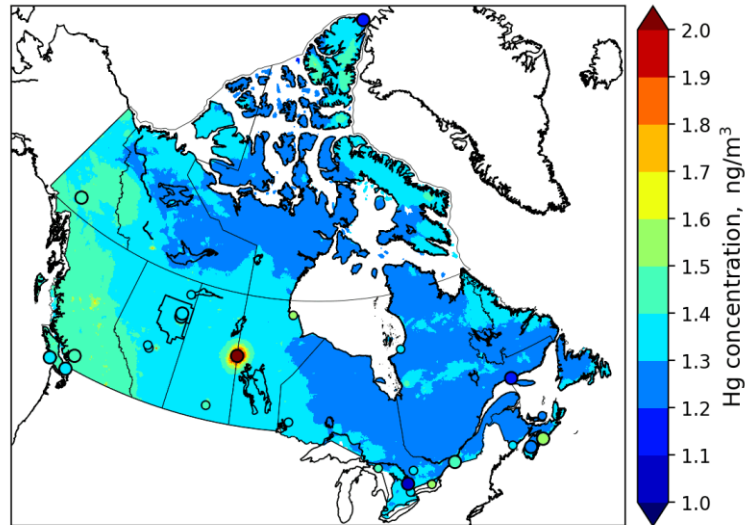
487  
 488 Figure 5: Simulated and observed surface air TGM concentrations in AOSR for the site Lower  
 489 Camp (2012—2014). Obs – observations; Mod – model estimation; BBE – modeled biomass  
 490 burning contribution.  
 491



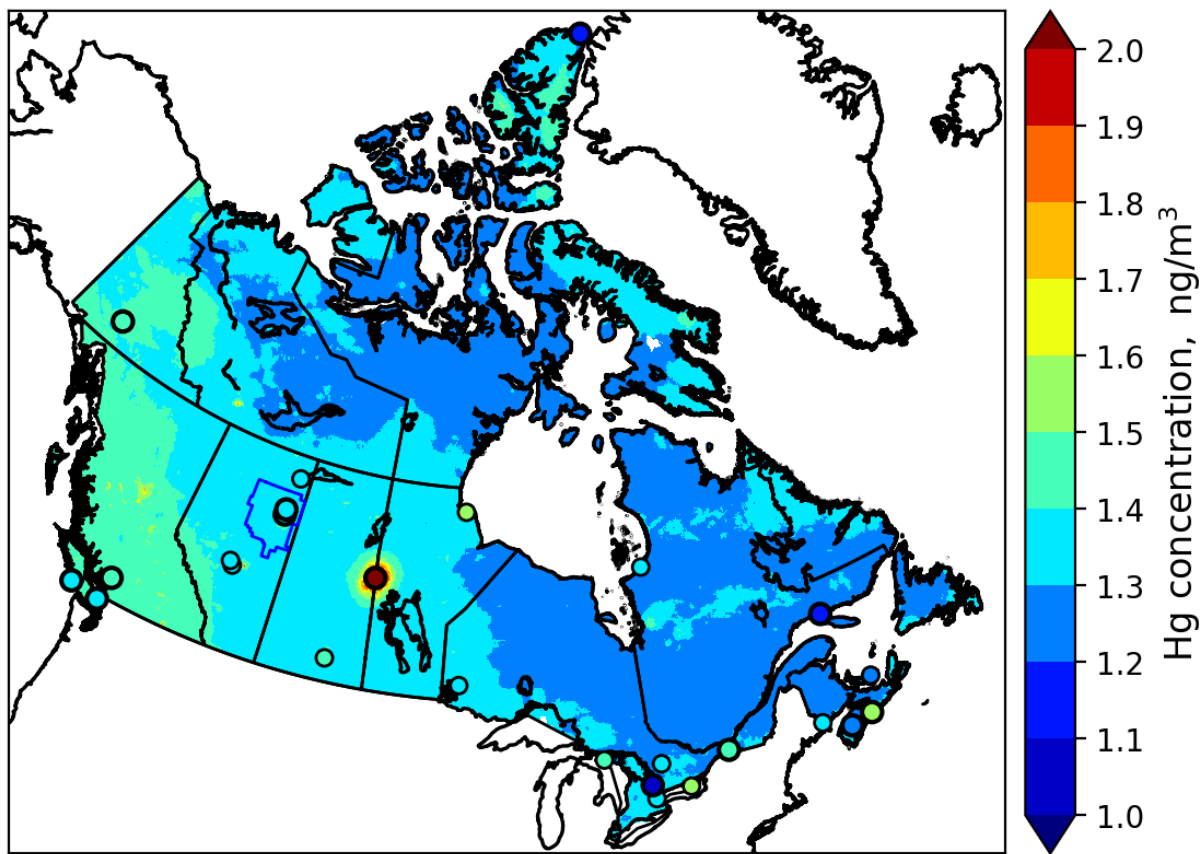
492  
 493 Figure 6: Simulated and observed surface air TGM concentrations in AOSR for the site Fort  
 494 McKay (2014 and 2015). Obs – observations; Mod – model estimation; BBE – modeled biomass  
 495 burning contributions.  
 496

497 For the purpose of comparing ambient GEM concentrations in the AOSR with other Canadian  
 498 regions, Figure 7 provides a map of modeled annual average surface air Hg concentrations of GEM  
 499 for Canada in 2013. In general, model estimated surface air GEM concentrations agreed well with  
 500 available observations (in circles), including western Canada, the Pacific coast, and the AOSR.  
 501 There is a general gradient in GEM concentrations from higher concentrations in the west (1.5 ng  
 502 m<sup>-3</sup>) to lower concentrations in the east (1.3 ng m<sup>-3</sup>). The average air concentrations of GEM in  
 503 the AOSR (1.40 ng m<sup>-3</sup>, 2012-2015) reflected the background GEM levels in Canada. The  
 504 simulated large-scale pattern in GEM concentrations is consistent with, and reflects, a dominant  
 505 role of trans-Pacific transport of GEM from East Asian Hg sources into Canada and the high  
 506 Arctic. GEM concentrations are slightly higher in major urban centres and regions of current and  
 507 past anthropogenic activities such as energy production from coal-fired power plants and mining.  
 508 The hotspot in Figure 7 near the Saskatchewan/Manitoba border is the former copper-zinc smelter

509 near Flin-Flon, MB, which ceased operations in 2010 (Ma et al., 2012). The soils in the  
510 surrounding region remain heavily contaminated with Hg. The re-emission of accumulated legacy  
511 mercury in soils (Eckley et al., 2013) is responsible for the highly elevated GEM concentrations  
512 in air.



513  
514

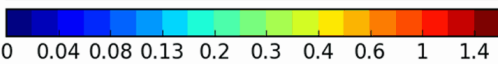
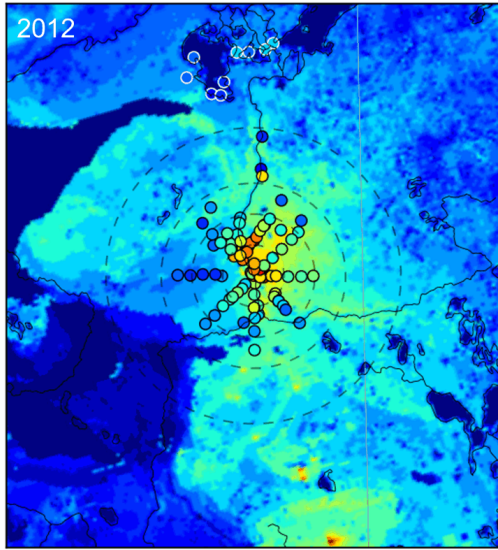


515  
 516 Figure 7: Model simulated spatial distribution of annual average surface air GEM concentrations  
 517 in Canada in 2013; colors in circles show observed concentrations for 2013 (large circles) and  
 518 previous years (small circles).

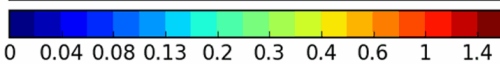
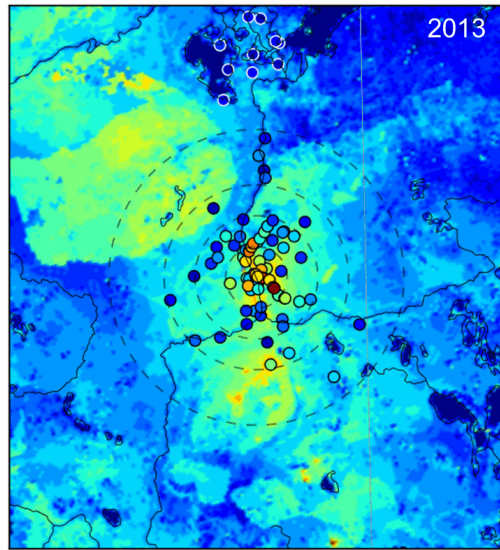
519  
 520 **Evaluation of model simulated mercury accumulation in snow**  
 521 Figure 8 compares total Hg loadings in snow simulated by the model with observations (in circles)  
 522 at the end of winter for years 2012-2015 in the AOSR. Cooke et al., (2017) used dated lake  
 523 sediment cores to reconstruct deposition trends and anthropogenic enrichment in the region, but  
 524 several correction factors needed to be applied to estimate Hg deposition fluxes and only two lakes  
 525 were cored in the direct vicinity of oil sands operations. By comparison, seasonal snowpack Hg  
 526 data provide the distribution of net total Hg deposition in the region with a large number of  
 527 sampling sites a short distance (< 25 km) away from sources. However, it should be noted that Hg  
 528 deposition in the snow is partially reduced and reemitted as well as adsorbed in surface soils due  
 529 to diffusion and intra-seasonal melt; therefore, snowpack Hg represents the lower limit of net

530 wintertime deposition. Observations at the sampling sites close to sources had the highest  
531 snowpack Hg loadings with decreasing concentrations as one moves further away from the  
532 immediate source region; the same spatial pattern was predicted by the model, and is most evident  
533 for the years with the largest emissions (2012 and 2013; Figure 8). Snow Hg contents at the  
534 background sites in the Peace Athabasca Delta region in the north were significantly lower, which  
535 was also well reproduced by the model. The figure shows high spatiotemporal variability in snow  
536 Hg loadings, which are related to changes in meteorological factors as well as oil sands emissions  
537 (as discussed later). The decline in both snowfall amounts and oil sands emissions led to lower  
538 snow Hg loadings in 2014 and 2015. Figure 9 shows the model simulated average snow depths in  
539 the AOSR and the observed depths at the Mildred Lake site close to the Syncrude upgrader. The  
540 model simulates snow amounts and interannual variations accurately. The model-estimated  
541 seasonal snow accumulations were 62, 183, 104 and 71 cm between October to May in 2012, 2013,  
542 2014 and 2015, respectively. An intense intra-seasonal melting event at the end of February was  
543 predicted by the model in each year, which is inline with observations. The largest melting event  
544 occurred in 2015, which caused over half of the snow accumulation to melt, and, thus, loss of half  
545 of seasonal snowpack Hg loadings. Modeled snow Hg loadings are in agreement with Gopalapilla i  
546 et al. (2019), who reported a temporal decrease in snow Hg loadings near-field (< 8 km from AR6),  
547 from an average load of 510 ng/m<sup>2</sup> in 2008 to 175 ng/m<sup>2</sup> in 2016. Relative importance of inter-  
548 annual changes in meteorological conditions and oil sands emissions to wintertime Hg deposition  
549 is discussed a later section.

550

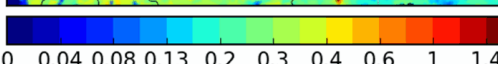
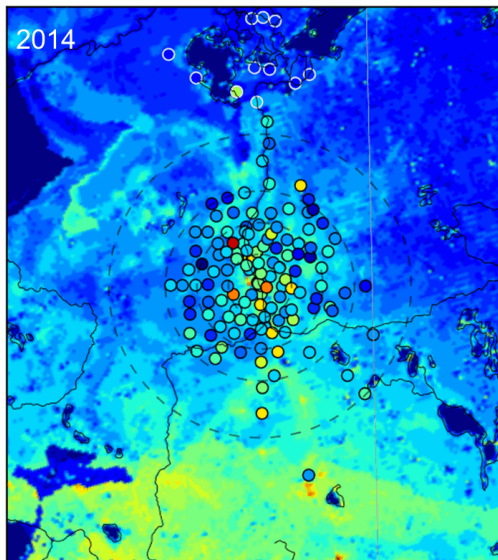


Hg accumulation in snow,  $\mu\text{g}/\text{m}^2$

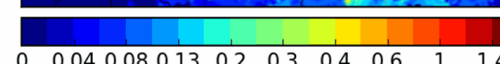
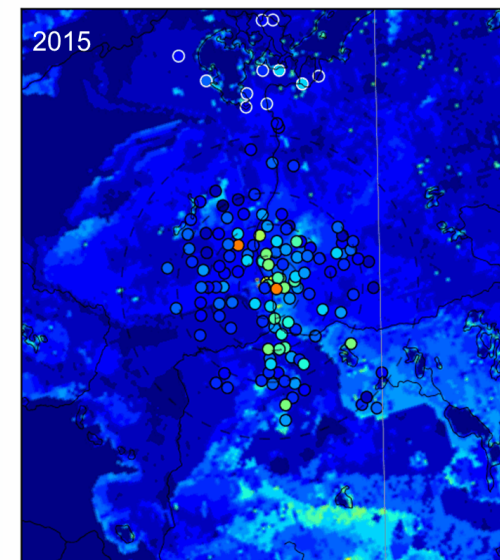


Hg accumulation in snow,  $\mu\text{g}/\text{m}^2$

551



Hg accumulation in snow,  $\mu\text{g}/\text{m}^2$



Hg accumulation in snow,  $\mu\text{g}/\text{m}^2$

552

553

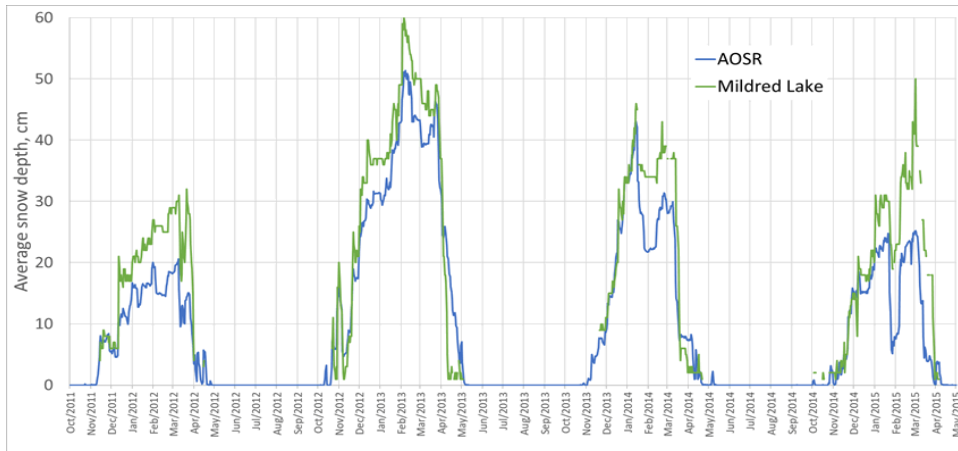
554

555

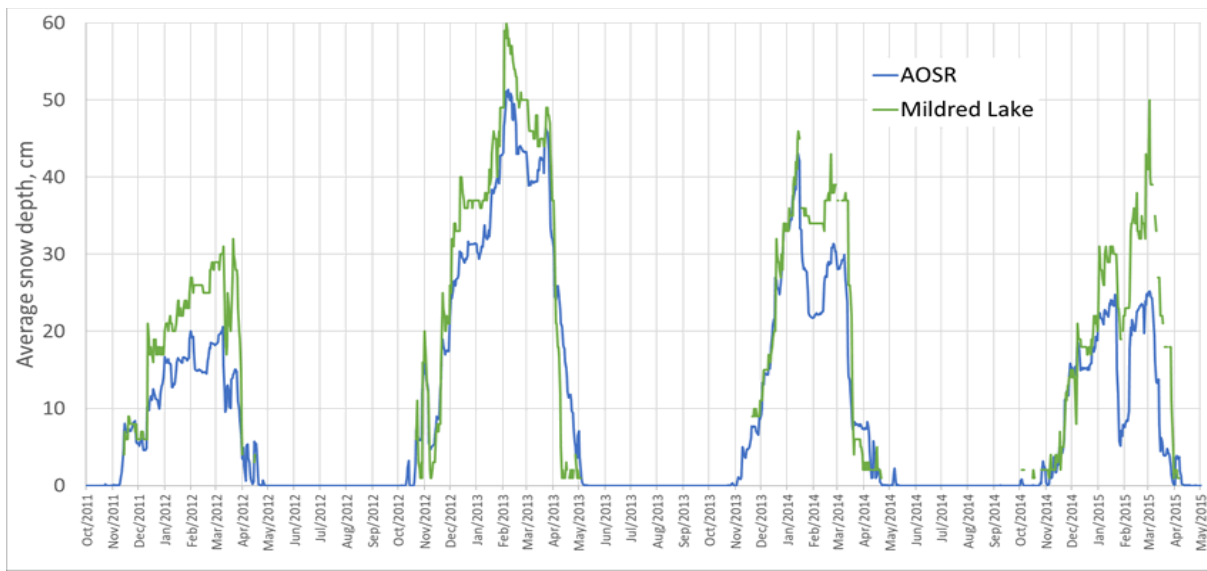
Figure 8: Seasonally accumulated Hg loadings in snow in AOSR from 2012 to 2015: modeled (background map) and observed values (colors in circles). Circles radii: 25, 50, 75, 120 km.



556



557



558 Figure 9: Daily averaged model simulated (blue) and observed snow depths (green) (cm) in 2012-  
559 2015 in the AOSR. Modeled values are averaged over the entire AOSR domain and the observation  
560 site is Mildred Lake, Alberta, a few km east of the Syncrude oil sands upgrader.

561

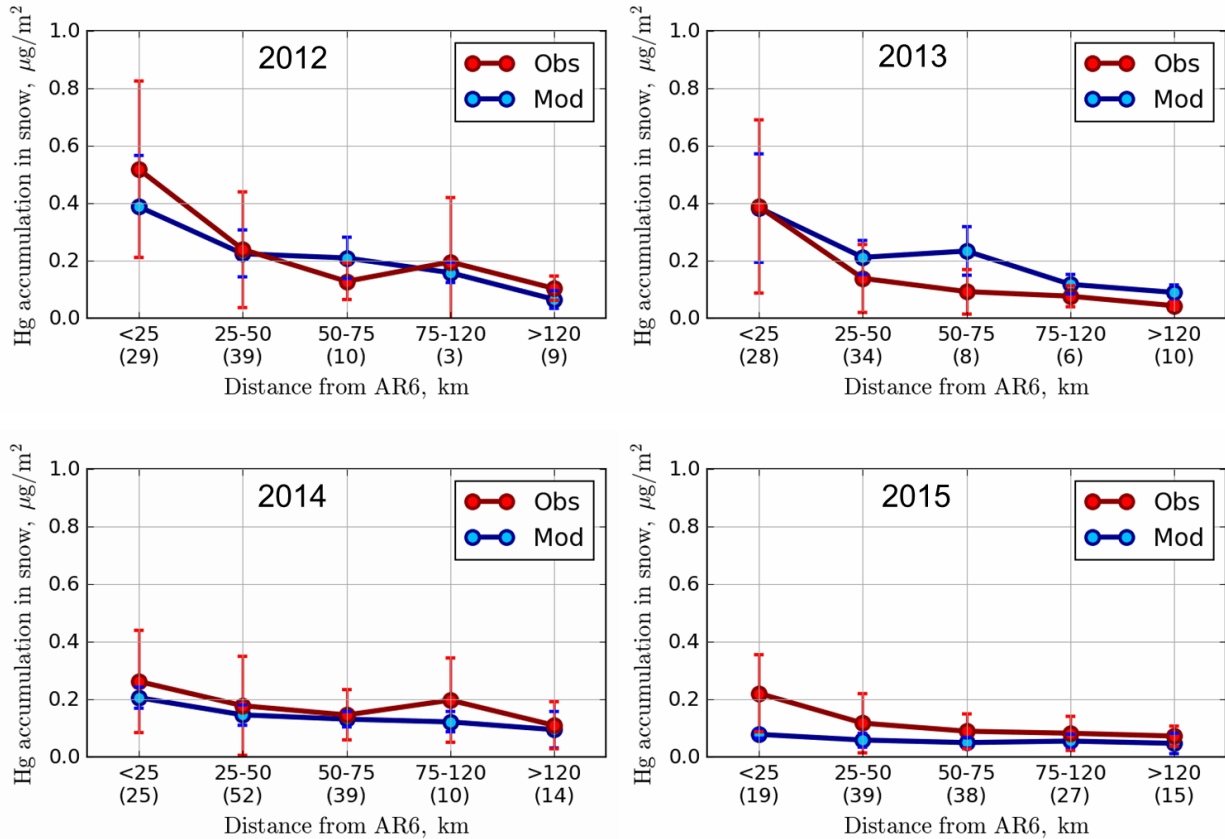
562 Figure 10 compares average modeled and observed snow Hg loadings at the sampling locations  
563 within 25 km, 25-50 km, 50-75 km, 75-120 and > 120 km distances from AR6. Inter-annual  
564 changes in meteorology and oil sands emissions led to decreases in total Hg loads from  $0.52 \pm 0.21$   
565 to  $0.22 \pm 0.09 \mu\text{g m}^{-2}$  within 25 km of AR6 (from 2012 to 2015) in the snowpack for observation  
566 and from  $0.39 \pm 0.21$  to  $0.08 \pm 0.06 \mu\text{g m}^{-2}$  for model estimates sampled at sites. The snow Hg  
567 loadings of up to  $0.7 \mu\text{g m}^{-2}$  were simulated by the model in the immediate vicinity of Hg emitting  
568 sources for 2012 (Figure 8). Emitted amounts of Hg from oil sands facilities were reported to the  
569 NPRI with the caveat that not all emissions, e.g., emissions of mercury that are part of fugitive



570 dust releases, are captured by the inventory. Brief episodes of Hg on larger particles (2.5-10  $\mu\text{m}$   
571 size) were observed at Fort McKay in late winter, likely originating from fugitive dust in the  
572 AOSR. These possible sources of Hg emissions and related deposition (in the vicinity of sources)  
573 were not included in the model. At  $> 120$  km from AR6, snowpack loadings were very low for all  
574 years at  $< 0.1 \mu\text{g m}^{-2}$  with small inter-annual variability, and indicate background Hg  
575 concentrations at this distance.

576  
577 While the strong decrease away from the source is mirrored in Figure 10 for the years 2012 and  
578 2013 (dropping from about  $0.4 \mu\text{g m}^{-2}$  at sites located  $< 25$  km from AR6 to  $< 0.1 \mu\text{g m}^{-2}$  at sites  $>$   
579  $120$  km away), the weaker signature from Figure 8 for the years 2014 and 2015 is more clearly  
580 represented in Figure 10, consistent with declines in reported oil sands emissions (see Table 1 and  
581 Figure 3). Modeled snow Hg loadings closer to the oil sands sources were lower compared to  
582 observed values in 2015. A sensitivity model simulation was conducted for 2015 by replacing  
583 NPRI reported Hg emissions from oil sands facilities in 2015 with 2014 values. The sensitivity  
584 model simulation matched the observed Hg loadings in the snow in 2015 at all distances; these  
585 results suggest that either NPRI Hg emissions from oil sands facilities were slightly under-  
586 represented or there was an unaccounted area source (such as from fugitive dust) of Hg in 2015.

587  
588 Model estimates and observations agreed well for all distances evaluated, and demonstrate the  
589 model's ability in correctly simulating the impacts of changes in Hg emissions and  
590 physicochemical processes in the cryosphere. The high variability in the observed snowpack data  
591 within  $50$  km of AR6 indicates that there are likely other local sources around mining facilities  
592 that impact local deposition (such as fugitive dust from coke pile and roads). However, modeled  
593 estimates at sampling locations agreed with observed snow Hg loadings within one standard  
594 deviation, and suggest that unaccounted sources of Hg do not have a significant impact on  
595 deposition in the AOSR, likely due to their episodic nature as suggested by observed ambient  
596 concentrations of particle-bound mercury.



597

598

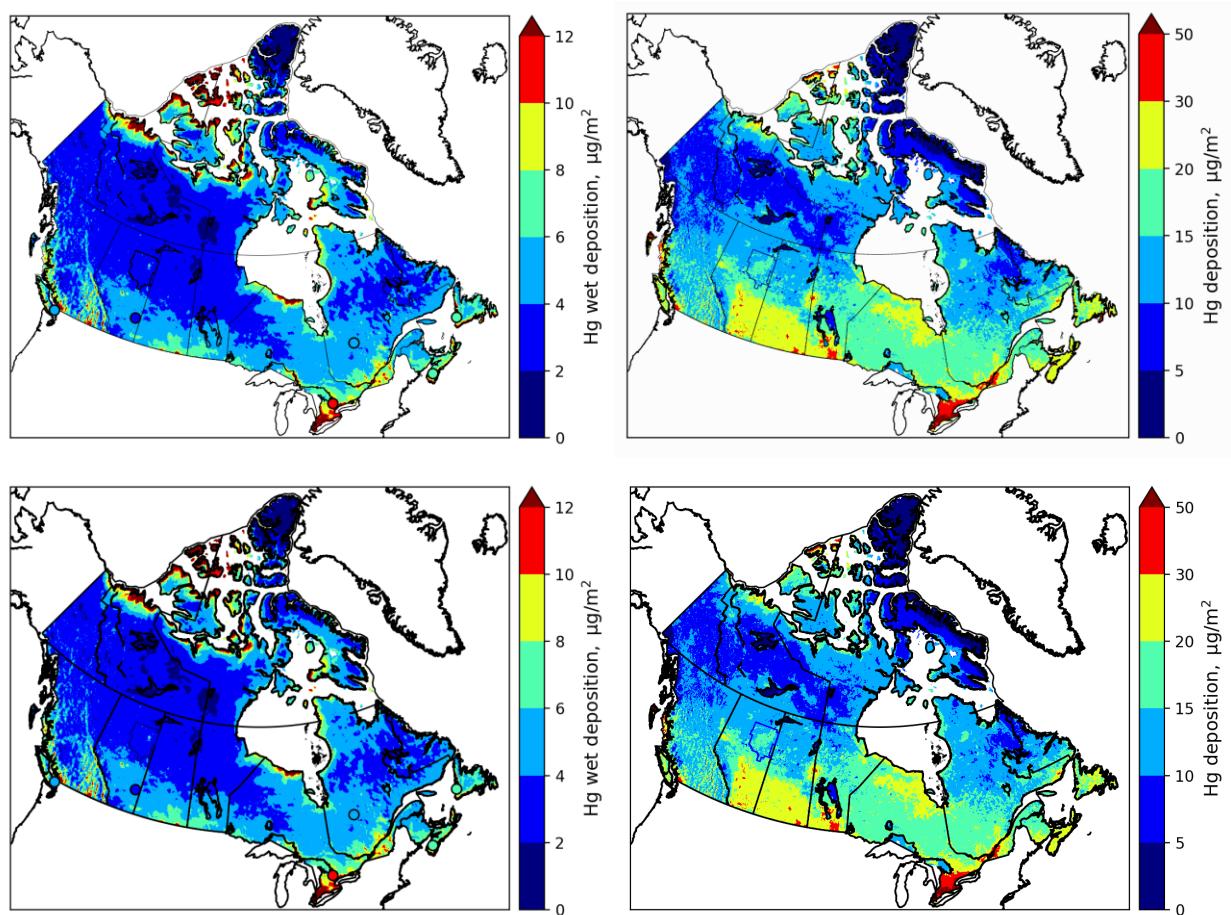
599 Figure 10: Average modeled ( $\mu\text{g m}^{-2}$ ; blue) and observed ( $\mu\text{g m}^{-2}$ ; red) end of winter Hg loadings  
600 in snowpack within 25 km, 25-50 km, 50-75 km and 75-120 and > 120 km distances from AR6  
601 along with  $\pm$ one standard deviations. Modeled accumulated Hg in the snow was sampled at the  
602 observation sites. Numbers in parentheses provide number of observation sampling sites in each  
603 distance cluster.

604

605 Comparison of modeled annual wet and total deposition (wet plus dry deposition) fluxes of Hg in  
606 the AOSR with other locations in Canada is presented in Figure 11 for 2013. In general, spatial  
607 distributions of wet and total deposition fluxes followed patterns of precipitation (high in the east,  
608 south and mountainous regions of Canada), industrial activities (high in southern Canada),  
609 vegetation density (boreal and temperate forests) as well as Hg transport from the US (higher in  
610 the east). Figure 11 shows good agreement with observed wet deposition fluxes (noted in circles)  
611 in coastal (Saturna Island, BC), rural (Southern Alberta) and urban areas (Egbert, ON). While  
612 direct measurements of annual total deposition fluxes are not available, the distribution of Hg  
613 deposition fluxes in Canada was found to be consistent with Canada-wide lake sediment inferred

614 deposition fluxes (Muir et al. 2009). Average annual total deposition fluxes in the AOSR were  
615 16.9, 15.7, 18.3 and 17.5  $\mu\text{g m}^{-2}$  in 2012, 2013, 2014 and 2015, respectively, slightly higher than  
616 in the other regions of northern Alberta ( $\sim 14 \mu\text{g m}^{-2}/\text{y}$ ) and lower than average Hg deposition flux  
617 in southern Alberta ( $\sim 25 \mu\text{g m}^{-2}/\text{y}$ ). The highest deposition up to  $80 \mu\text{g m}^{-2}$  occurred in southern  
618 Ontario in Canada due to the presence of local anthropogenic mercury emissions in these regions.

619



620

621

622 Figure 11: Model simulated and observed annual Hg wet deposition for 2013 (left) (colors in  
623 circles show observed wet deposition for 2013) and simulated annual total Hg deposition (right)  
624 (wet plus dry deposition) in Canada for 2013.

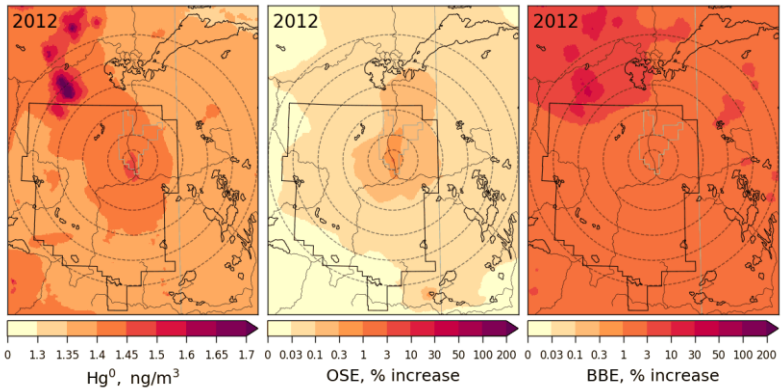
625

### 626 **Impacts of oil sands developments and wildfires on mercury levels in air and deposition**

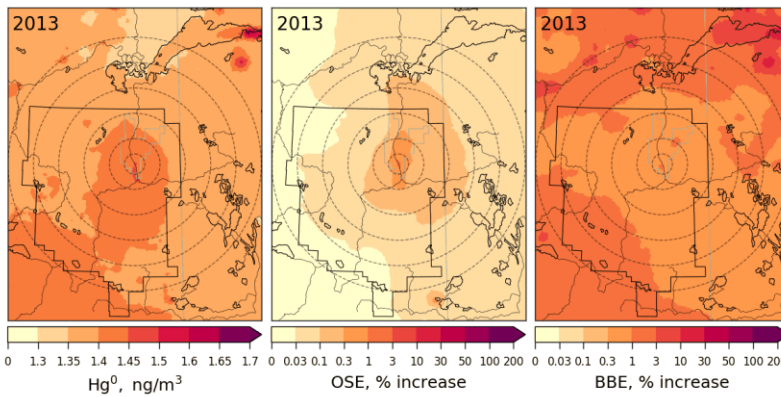
627 Employing GEM-MACH-Hg, the impacts of Hg emissions from oil sands developments in the  
628 AOSR on surface air concentrations of Hg species (i.e., GEM and TOM), snowpack Hg loadings,  
629 and annual Hg deposition were investigated for the years 2012-2015. Since Northwest Canada is

630 a region of high wildfire activity (Fraser et al. 2018), the relative role of Hg emissions from  
631 biomass burning in North America on the Hg burden in the AOSR was also examined.

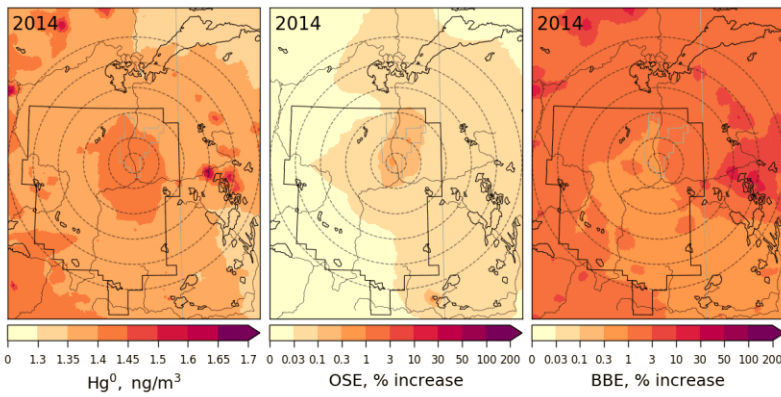
632 Figures 12 & 13 provide spatial distributions of simulated annual average surface air  
633 concentrations of GEM (globally transported and the dominant ambient Hg species) and TOM  
634 (regionally transported and efficiently deposited Hg species) (left panels) for the years 2012 to  
635 2015 along with their contributions (as % increases) from oils sands emissions (OSE, middle  
636 panels) and biomass burning emissions (BBE, right panels) in the AOSR and the surrounding  
637 region. GEM air concentrations were  $1.4 \text{ ng m}^{-3}$  in the AOSR in 2012-2015, which is within the  
638 range of GEM concentrations observed in Alberta (i.e.,  $1.2\text{-}1.5 \text{ ng m}^{-3}$  in 2012). While annual  
639 average GEM concentrations were slightly elevated close to the major upgraders ( $> 1.5$  within 5  
640 km vs  $1.4 \text{ ng m}^{-3}$  200 km away from AR6) in the AOSR, GEM concentrations were found to be  
641 elevated up to  $1.8 \text{ ng m}^{-3}$  in surrounding regions of the AOSR due to local wildfires in 2012-2015.  
642 Since the lifetime of GEM in the air is between 0.5-1 year, GEM concentrations are largely driven  
643 by global transport in the AOSR (and Canada) with only minor contributions from local emissions.  
644 Oil sands emissions increased atmospheric GEM concentrations up to 2.3% in 2012 and 2013, and  
645 negligibly (up to 0.9%) in low OSE years 2014-2015, only very close to the upgraders (i.e., within  
646 2.5 km). Wildfire activities are highly variable from year to year, and can significantly impact  
647 GEM concentrations in the AOSR in summertime (Fraser et al. 2018). Biomass burning  
648 contributed to 1.0-2.2% increases in average GEM concentrations in and around the AOSR (Figure  
649 12, right panels), making biomass burning a more important source of GEM than OSE in the  
650 region. Strong regional biomass burning events led to large increases in GEM concentrations of  
651 up to 35% (2012-2015) in the AOSR and the surrounding regions.



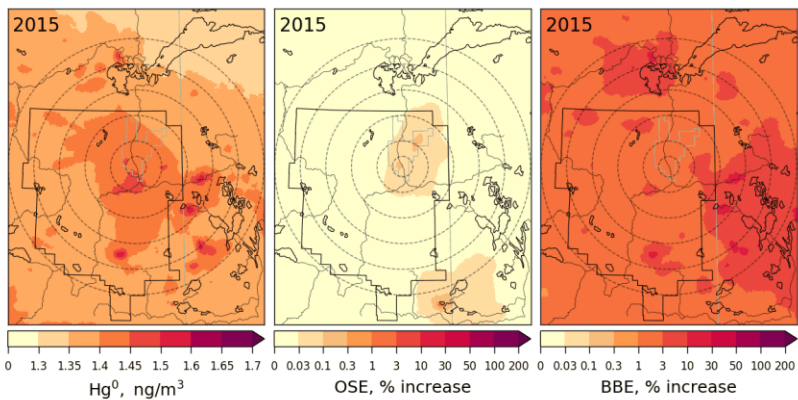
652



653



654



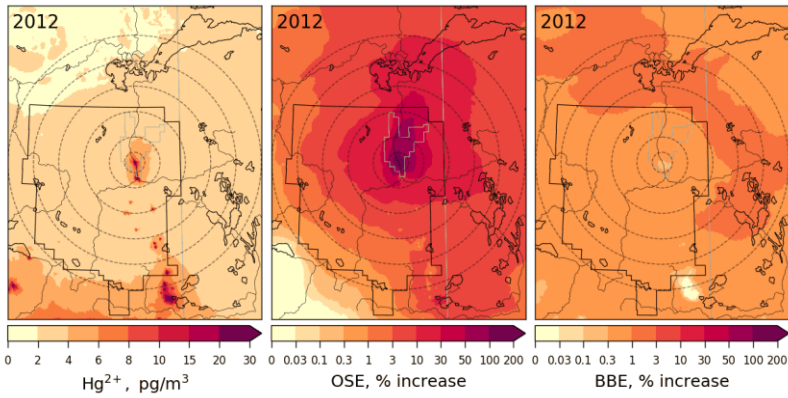
655

656 Figure 12: Annual average surface air concentration of GEM (left) and concentration enrichments  
657 (%) due to Hg emissions from Athabasca oil sands operations (OSE, middle) and biomass burning  
658 in North America (BBE, right) for the years 2012 to 2015. The AOSR is marked as an approximate  
659 rectangle, and concentric distance circles are at 20, 50, 100, 150, 200 and 250 km from AR6.

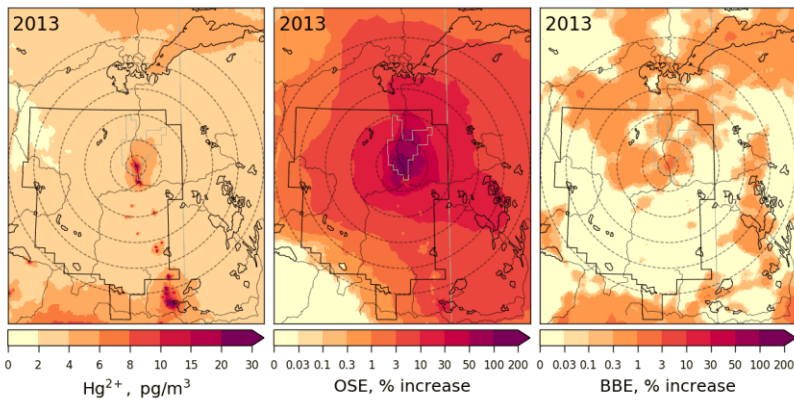
660  
661 While average surface air TOM concentrations in the AOSR were only  $3.3 \text{ pg m}^{-3}$  (consistent with  
662 observations), hot spots were modelled in the immediate vicinity of the major upgraders ( $> 25 \text{ pg}$   
663  $\text{m}^{-3}$  within 5 km from AR6 in 2012-2013) in the AOSR (Figure 13, left panels). In 2014-2015,  
664 TOM concentrations around AR6 were about half of 2012-2013 ( $12 \text{ pg m}^{-3}$ ), consistent with  
665 reported changes in Hg emissions from the respective facilities. OSE are found to be the main and  
666 a major contributor of oxidized Hg concentrations in surface air close to oil sands sources,  
667 increasing background concentrations over 30% within 100 km and 60% within 50 km from AR6  
668 in 2012-2013, particularly in the northeast sector of the AOSR. Wildfire emissions played a minor  
669 role in ambient TOM concentrations in the region, contributing to  $< 1\%$  increases in 2012, 2013  
670 and 2015, but increased to  $\sim 6\%$  in 2014 as a result of higher wildfire activities. Hg emitted from  
671 oil sands operations as oxidized species is deposited efficiently by precipitation and uptake from  
672 terrestrial surfaces in the vicinity of the sources. By comparison, most of the GEM emissions are  
673 transported out of the region except for a small fraction being deposited locally via direct  
674 vegetation uptake and conversion to oxidized species and dry deposition. Oxidized Hg species  
675 emitted from global sources do not reach the AOSR via long-range transport due to their short-  
676 lived nature. As a result, OSE-related Hg deposition in the AOSR consists primarily of TOM,  
677 whereas, long-range transport of GEM accounts for the deposition in the AOSR attributed to  
678 outside sources. Wildfire emissions are mostly assumed to be emitted as GEM as indicated by  
679 observations (Friedli et al. 2001).

680

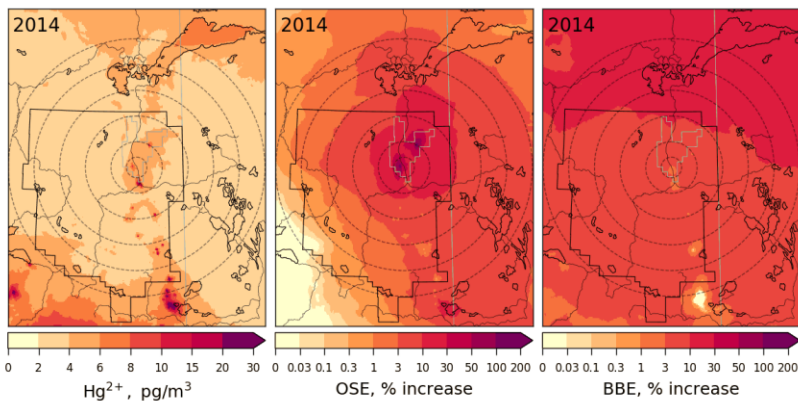




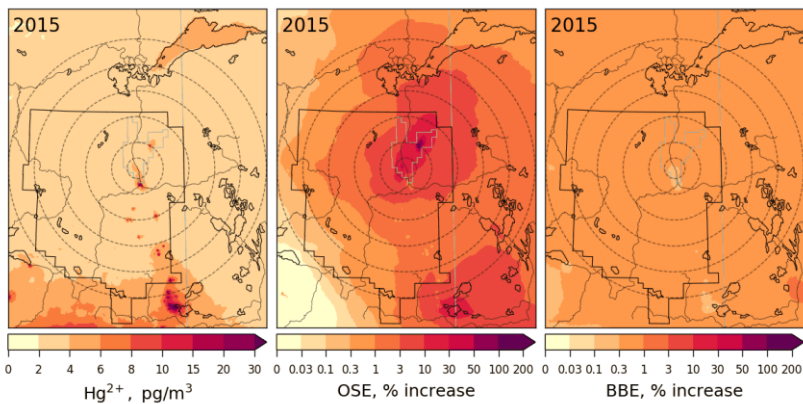
681



682



683



684

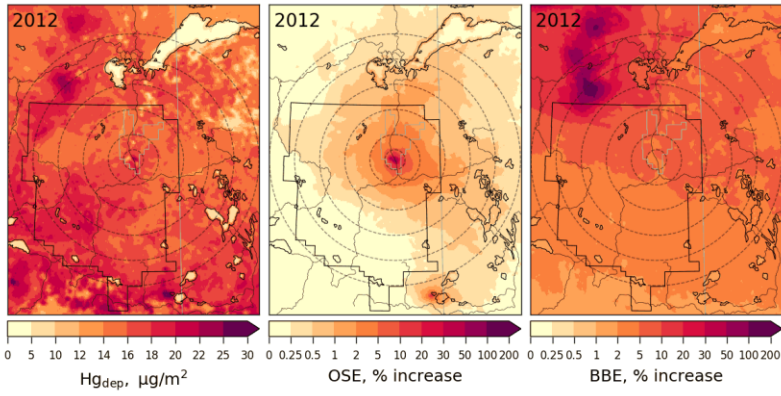


685 Figure 13: Annual average surface air concentration of TOM (sum of GOM and PBM, left), and  
686 concentration enrichments (%) due to Hg emissions from Athabasca oil sands operation (OSE,  
687 middle) and biomass burning in North America (BBE, right) for the years 2012-2015. AOSR is  
688 marked as an approximate rectangle and concentric distance circles are at 20, 50, 100, 150, 200  
689 and 250 km from AR6.

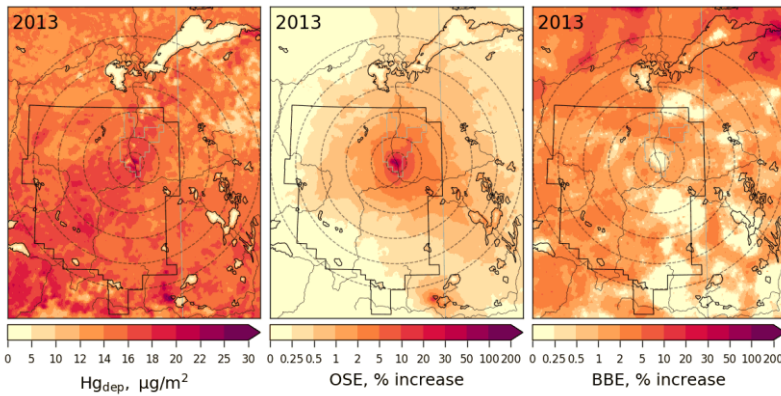
690  
691 Figures 14 and 15 provide spatial distributions of modelled annual total mercury deposition (Figure  
692 14, left panels) and seasonally accumulated Hg loadings in the snow (Figure 15, left panels), and  
693 their source attributions to OSE (Figure 14, middle panels; Figure 15, right panels) and BBE  
694 (Figure 14, right panels) in the AOSR in 2012-2015. Mercury deposition fluxes from 7-28  $\mu\text{g m}^{-2}\text{y}^{-1}$   
695 ( $15.6 - 18.3 \mu\text{g m}^{-2}\text{y}^{-1}$ , averages) were modelled in the AOSR in 2012-2015, originating from  
696 all Hg emission sources - global primary and legacy anthropogenic and geogenic (including oil  
697 sands and biomass burning) emissions. Since the contribution of global transport of GEM to the  
698 ambient total Hg concentrations in the AOSR is much larger than the contributions of OSE and  
699 BBE (Figure 12) and GEM concentrations are typically 2-3 order of magnitude higher than TOM  
700 concentrations (which have higher contributions from OSE, Figure 13), deposition of imported  
701 GEM makes up a major portion of the annual Hg deposition in the AOSR on a broad spatial scale,  
702 despite its lower Hg deposition efficiencies than TOM (Figure 14). Similar to ambient TOM  
703 concentrations, modelling reveals the impact of OSE to Hg deposition to be greatest in the vicinity  
704 of upgraders, i.e., average increases of 17%, 20%, 8%, and 3% within 20 km of AR6 in 2012,  
705 2013, 2014 and 2015, respectively, and < 1 % beyond 50 km in all years. Model results reveal a  
706 larger impact of OSE on Hg deposition in the regions northeast of oil sands sources, consistent  
707 with observations and prevailing wind direction and speed (Kirk et al. 2014). Average Hg  
708 deposition contributions due to BBE (increases of 1.4-13% ) were higher than OSE contributions  
709 (increases of 0.3-1.3%) across 200 km of oil sands operations in 2012-2015. Wildfires in the  
710 region led to localized increases in Hg deposition of up to 193% and 101% in 2012 and 2014,  
711 especially northwest of the AOSR. Mercury emissions from electricity generation in southern  
712 Alberta accounted for a general decrease in Hg deposition fluxes from south to north around the  
713 AOSR.

714

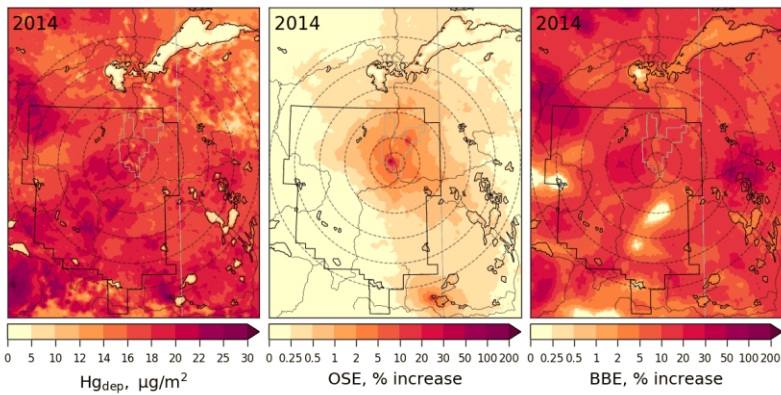
715



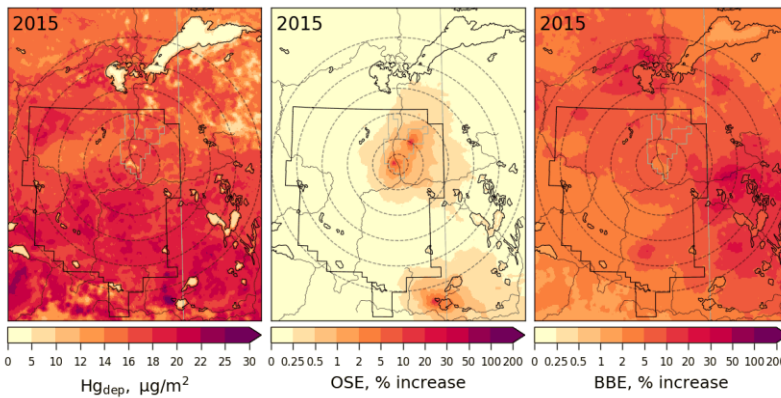
716



717



718



719

720 Figure 14: Annual total Hg deposition flux (left) and deposition enrichments (%) due to Hg  
721 emissions from Athabasca oil sands operations (OSE, middle) and biomass burning in North  
722 America (BBE, right) in 2012-2015. The AOSR is marked as an approximate rectangle and  
723 concentric distance circles are at 20, 50, 100, 150, 200 and 250 km from AR6.

724  
725 Snowpack Hg accumulations from the start of the snow season to the end of winter (roughly  
726 coinciding with the maximum snow accumulation period) and their contributions from oil sands  
727 Hg emissions were estimated for 2012-2015 (Figure 15). Background snow Hg loadings (without  
728 the impact of OSE, middle panels) were spatially highly variable (up to  $1.4 \mu\text{g m}^{-2}$ ) in the region  
729 between 2012-2015. The higher snow Hg background levels resulted from both the regional  
730 transport of Hg from southern Alberta as well as spatial inhomogeneity in the accumulation of  
731 snow. Closer to OSE sources, total Hg loadings in snow reached up to  $1.0 \mu\text{g m}^{-2}$  (< 20 km from  
732 AR6) in 2012-2014 (Figure 15). In 2015, emissions from oil sands-related activities were the  
733 lowest and total Hg loadings corresponded to background emissions. The impact of OSE was  
734 notably greater to the snowpack Hg loadings, including the spatial extent, than to the annual Hg  
735 deposition (Figure 15, right panels). Average increases of 55%, 43%, 35% and 7% in snow Hg  
736 amounts were simulated within 50 km of AR6 in 2012, 2013, 2014 and 2015, respectively, as a  
737 result of OSE. Regions northeast of the AOSR showed increases of 27-44% in snow Hg levels in  
738 2012 and 2013 and 3-24% in 2014 and 2015 between 50-100 km from AR6. Model results support  
739 the conclusions of previous studies that oil sands Hg emissions have a large impact on snow Hg  
740 loadings near the oil sands emission sources with decreasing contributions away from AR6 (Kelly  
741 et al., 2010; Kirk et al., 2014). The distinctive pattern of higher snow Hg loadings in the northeast  
742 region surrounding the AOSR was also reported (Kirk et al., 2014). Model results reveal high  
743 spatiotemporal variability in background snow Hg loadings; this is related to variability in snowfall  
744 amounts, meteorological conditions affecting melting and snowpack Hg processes including  
745 redox, air-snow exchange and transport to soils.

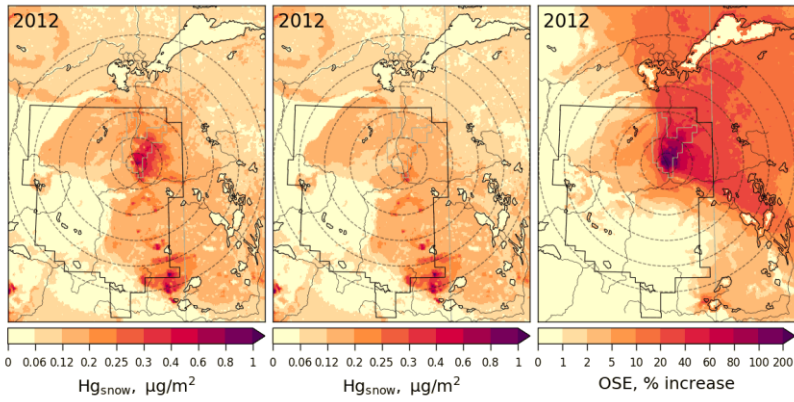
746  
747 Average annual Hg deposition fluxes in the AOSR were 13.3 (2015) to 18.5 (2013)  $\mu\text{g m}^{-2}\text{y}^{-1}$   
748 within 10 km, 15.0 (2015) to 16.9 (2013)  $\mu\text{g m}^{-2}\text{y}^{-1}$  between 10-20 km, and  $\sim 16 \mu\text{g m}^{-2}\text{y}^{-1}$  50 km  
749 away from the major oil sands emission sources. In the AOSR, winter (and snow cover) can last  
750 up to six months (from November to April) with maximum snow depths in January-February.

751 Winter (November-April) and summer (June-August) periods contributed to ~20% and 50%,  
752 respectively, of annual Hg deposition in AOSR. In Figure 16, three representative months in the  
753 winter (December to February) and summer (June to August) seasons, each, are chosen to present  
754 the inter-seasonal contrast in OSE impacts on Hg deposition along with the impact on annual  
755 deposition as a function of distance from AR6.

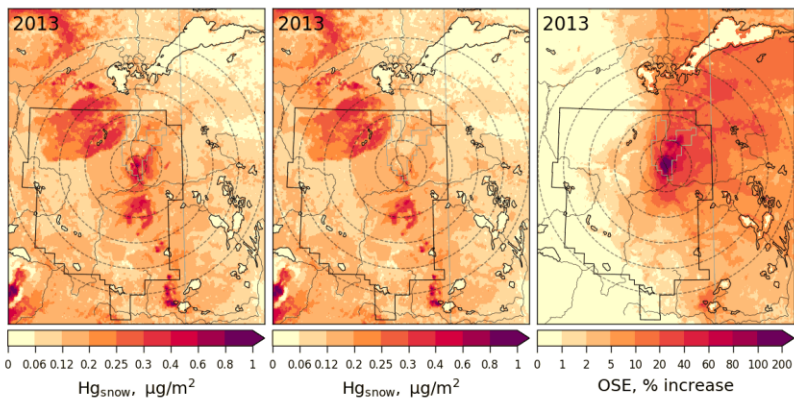
756  
757 Seasonally, OSE accounted for the largest Hg deposition increases in winter months: ~230-500%  
758 (2013), 146-374% (2012), 94-104% (2014) and 40-43% (2015) within 10 km; 75% (2013), 57%  
759 (2012), 25% (2014) and 5% (2015) at 20 km; and 24-33% (2012-2013) and 6-12% (2014-2015) at  
760 50 km distance from the major oil sands upgraders. In summertime, lower deposition increases  
761 due to OSE were estimated, ~13-56% (2012-2013) and 3-7% (2014-2015) within 10 km, and <  
762 7% (2012-2015) at 20 km from AR6. Annually, OSE accounted for deposition increases of ~24-  
763 70% (2012-2013), 14% (2014) and <5% (2015) within 10 km, 10% (2012-2013) and <5% (2014-  
764 2015) at 20 km, and <4% (2012-2015) at 50 km from the major oil sands emission sources. These  
765 seasonal variations are consistent with inter-seasonal differences in Hg deposition pathways (i.e.  
766 the dominant role of GEM uptake by vegetation in summer from global sources, and uptake of  
767 local TOM emissions by snowfall and snowpack as the main pathway in wintertime deposition)  
768 (Graydon et al., 2006; Obrist et al., 2016; Zhang et al. 2009). The influence of OSE to summertime  
769 and annual depositions is also more limited spatially (up to 30 km of OSE) than to wintertime  
770 deposition (up to 100 km of OSE), consistent with observations (Kirk et al, 2014; Gopalapillai et  
771 al., 2019).

772

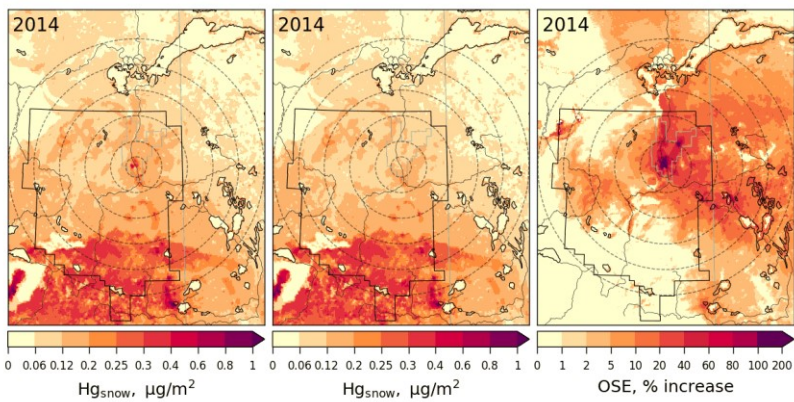
773



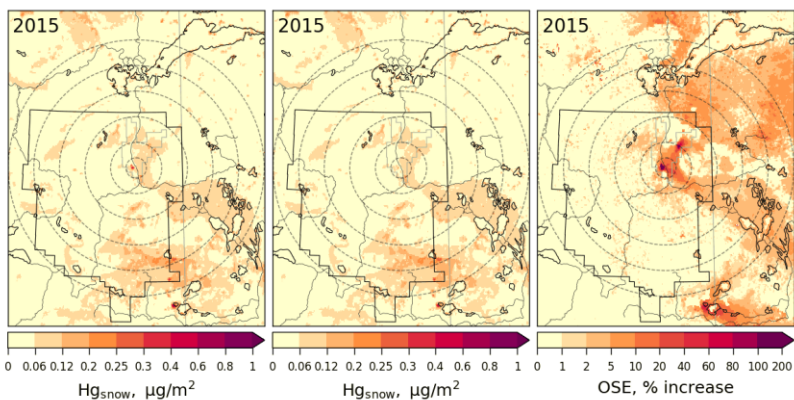
774



775



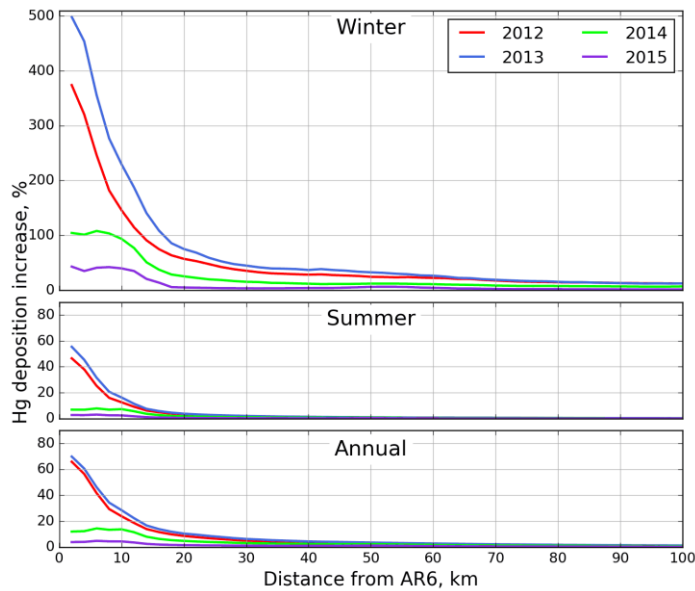
776



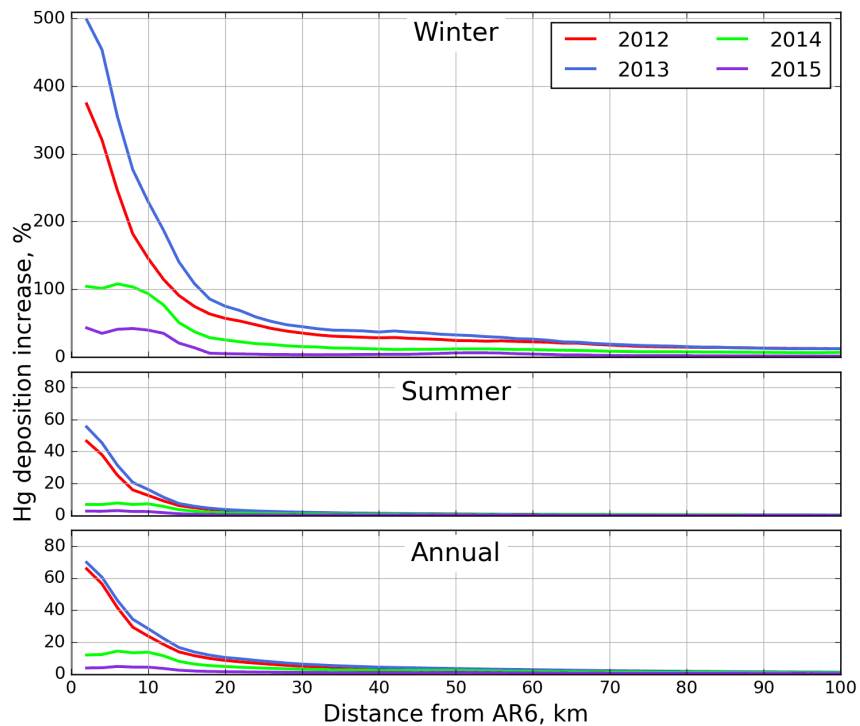
777

778 Figure 15: Seasonally accumulated Hg loadings in snow with all Hg emissions (left) and without  
 779 Athabasca oil sands Hg emissions (middle), and enrichments (%) in seasonally accumulated Hg  
 780 loadings in snow due to Athabasca oil sands Hg emissions (OSE, right) in 2012-2015. The AOSR  
 781 is marked as an approximate rectangle and concentric distance circles are at 20, 50, 100, 150, 200  
 782 and 250 km from AR6.

783



784



785



786 Figure 16: Average Hg deposition enrichments (%) due to Athabasca oil sands emissions in winter  
787 from December to February (top), in summer from June to August (middle), and annually (bottom)  
788 for 2012 (red), 2013 (blue), 2014 (green) and 2015 (pink) by distance from AR6.

789

### 790 **Process attribution of interannual variations in mercury deposition**

791 The interannual differences noticed in Figure 16 raises the question of the contributing factors to  
792 the interannual variability of Hg deposition in different seasons, especially close to the processing  
793 facilities (i.e., within a 10 and 20 km radius). The relative importance of variations in  
794 meteorological conditions and changes in OSE and BBE on the temporal changes in Hg deposition  
795 fluxes from 2012 to 2015 were analyzed. Since meteorological changes are expected to occur  
796 regardless of changes in emissions, a controlled model simulation was first conducted by applying  
797 only meteorological changes only from 2012 to 2015. Subsequently, two additional model  
798 simulations were performed by ~~including changes in BBE and OSE successively.~~ adding BBE  
799 and OSE changes from 2013-2015. The differences in these simulations provided the relative  
800 process contributions. It should be noted that ~~interannual variations,~~ in addition to the changes in  
801 emissions, the BBE and OSE impacts on Hg deposition also depend on changes in meteorological  
802 factors/conditions (synoptic as well as local scale) ~~affect overall seasonal and annual deposition~~  
803 ~~rates and, therefore, the magnitude of the impacts of various emissions on the deposition,~~  
804 ~~irrespective of the changes in emissions;~~ thus, the results presented here are cumulative  
805 contributions of changes in meteorology and emissions. Figure 17 presents process attribution of  
806 interannual changes in winter (top), summer (middle) and annual (bottom) Hg deposition rates  
807 from 2012-2015 within 0-10 km (left) and 10-20 km (right) from AR6. The lower panels illustrate  
808 Hg deposition source contributions from global emissions (green; global anthropogenic (except  
809 oil sands), geogenic and re-emission), OSE(red) and BBE(purple), and the upper panels show  
810 process contributions of changes in meteorology (blue), oil sands (red) and biomass burning  
811 (purple) emissions to interannual changes in total Hg deposition.

812

813 While wintertime Hg deposition fluxes were relatively low (2.6-3.6  $\mu\text{g m}^{-2}$ , November-April; 0.3  
814 – 0.8  $\mu\text{g m}^{-2}$ , December-February) in the AOSR, oil sands emissions were a major source of Hg  
815 deposition close to the oil sands sources as explained earlier, contributing to 70-80% of deposition

816 within 10 km of AR6 in high oil sands emission years (2012 and 2013). Wintertime (net) Hg  
817 deposition to northern landscapes is controlled by cryospheric processes, which exhibit strong  
818 interannual variations; therefore, interannual variation in wintertime Hg deposition is strongly  
819 controlled by meteorological conditions including snowfall amounts, wind speed, surface air  
820 temperature, solar insolation, and intra-seasonal melting affecting air-snow-soils exchange  
821 processes of mercury (Faïn et al., 2013). In 2015, a large snowmelt event at the end of February  
822 effectively removed about half of the accumulated mercury in snow resulting in much lower snow  
823 Hg content at the time of sampling (see Figure 9).

824  
825 Surface temperature and intra-seasonal melting have a large impact on how much of the deposited  
826 Hg in the snow is re-emitted back to the atmosphere and how much is adsorbed to surface soils,  
827 altering snow Hg loadings and net wintertime Hg deposition. Since 2013 experienced deeper  
828 snowpack and less inter-seasonal melting, a larger fraction of snowpack Hg was reduced and  
829 revolatilized, leading to a lower net Hg deposition despite slightly higher oil sands Hg emissions  
830 compared to 2012. Conversely, lower snowpack depth and a strong melting event at the end of  
831 February in 2015 allowed a large fraction of snowpack Hg to be transferred and retained in  
832 underlying soils increasing net Hg deposition, particularly the background deposition contribution.

833  
834 Within 10 km of major oil sands sources, wintertime variations in meteorology led to Hg  
835 deposition declines of 17% in 2013 and 2014 and increases of 10% in 2015 along with OSE-led  
836 deposition declines of 10% (2013), 35% (2014) and 56% (2015). When combined, the net effect of  
837 these two factors were overall reductions in wintertime Hg deposition fluxes of 27% (2013), 52%  
838 (2014) and 46% (2015), relative to 2012. At a distance of 10-20 km from the oil sands sources,  
839 changes in meteorology led to a 54% increase in wintertime Hg deposition in 2015, but the overall  
840 deposition only increased by 19%, because the decline in oil sands Hg emissions reduced the  
841 deposition by 35%. River discharge rates and Hg concentrations are reported to be highest in the  
842 spring meltwater flood (between 3 ng/L and 16 ng/L, up from typically <2 ng/L at their lowest  
843 annual level) in tributaries of the Athabasca River and pose risk to the downstream environments  
844 (Kelly et al., 2010; Wasiuta et al., 2019). Since the ground is still frozen at the time of spring  
845 freshet, Hg runoff is derived from seasonal snowpack loadings and mobilization of Hg from



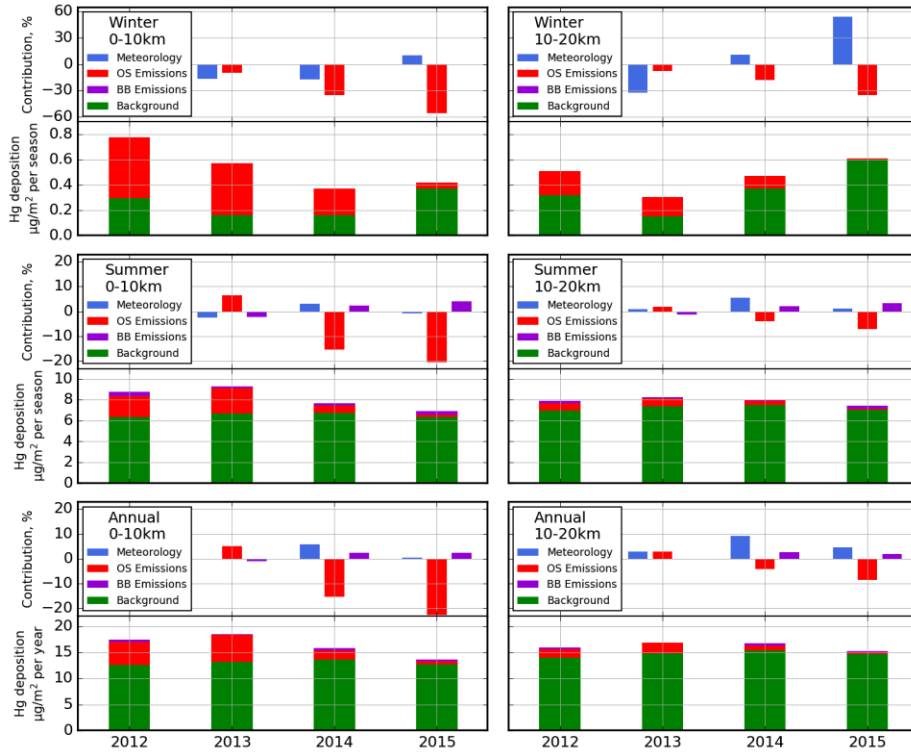
846 surface soils, both of which are contaminated by oil sands emissions in proximity of the sources  
847 and show a sensitivity to changes in Hg emissions from oil sands developments.

848  
849 Compared to winter, AOSR summertime background Hg deposition fluxes were significantly  
850 higher ( $\sim 6.3\text{-}7.5 \mu\text{g m}^{-2}$ , 2012-2015) and less variable in space and time, and OSE contributions to  
851 total deposition were relatively lower ( $\sim 0.05\text{-}0.5 \mu\text{g m}^{-2}$  within 10 km and  $0.01\text{-}0.2 \mu\text{g m}^{-2}$  from  
852 10-20 km, 2012-2015). In addition, summertime biomass burning emissions contributed to Hg  
853 deposition of  $0.1\text{-}0.4 \mu\text{g m}^{-2}$  (2012-2015). Summertime Hg deposition to terrestrial systems is  
854 temporally less variable than wintertime deposition as it is predominantly driven by Hg uptake by  
855 vegetation and soils followed by wet deposition. Changes in oil sands emissions played a more  
856 significant role than the meteorological factors in summertime inter-annual Hg deposition  
857 variations.. Compared to 2012, changes in meteorology, biomass burning and oil sand emissions,  
858 respectively, led to changes in summertime Hg deposition fluxes by -3%, -2%, and +7% in 2013,  
859 +3%, +2% and -15% in 2014, and -1%, +4% and -20% in 2015, resulting in overall changes in Hg  
860 deposition by +2% (2013), -10% (2014) and -17% (2015), within 10 km of major oil sands sources.  
861 Interannual variations in precipitation amounts and its impact on the wet deposition of Hg was the  
862 primary reason for the meteorology-related changes in summertime Hg deposition fluxes.

863  
864 Since summertime deposition contributes to about half of the annual deposition, interannual  
865 changes and their responsible factors in annual Hg deposition fluxes had a similar pattern as  
866 summer, with a relatively larger impact of changes in OSE on Hg deposition fluxes in the  
867 immediate vicinity of oil sands sources. Relative to 2012, deposition increases were 6 (2014) and  
868 1% (2015) due to variations in meteorology and 2% (2014-2015) due to biomass burning, and  
869 deposition declines were 15 (2014) and 23% (2015) due to reduction in oil sands Hg emissions.  
870 This results in overall reductions in annual Hg depositions of 7 (2014) and 20% (2015) within 10  
871 km of AR6. These model results demonstrate that reduction in Hg emisisions from oil sands  
872 processing activities lead to measurable declines in mercury deposition fluxes in AOSR. Further  
873 away from sources (right panel, Figure 17), the changes in meteorology and oil sands emissions  
874 resulted in comparable changes in Hg deposition rates (+9 (2014) and +5 % (2015), meteorology;  
875 -4 (2014) and -9% (2015), OSE) along with 3(2014) and 2(2015)% increases in deposition due to  
876 BBE, resulting in relatively smaller overall changes (+8% (2014) and -2% (2015)) in Hg deposition

877 fluxes. Interestingly, land clearing in the AOSR contributes to reduced background Hg deposition  
 878 fluxes due to the reduction in foliage Hg uptake; average background Hg deposition fluxes were  
 879 about  $1 \mu\text{g m}^{-2}$  lower within 10 km as compared to Hg deposition fluxes 20 km away from the  
 880 major oil sands activities.

881



882



883  
 884 Figure 17: (a) December – February, (b) June – August and (c) yearly averaged source  
 885 apportionment of total Hg depositions (lower panels) in 2012-2015, and contributions of changes  
 886 in meteorology, Athabasca oil sands emissions and biomass burning emissions (only in summer)  
 887 (top panels) to the changes in total Hg depositions in 2013-2015 relative to 2012, within 10 km  
 888 (left plot) & 10-20 km (right plot) of AR6.

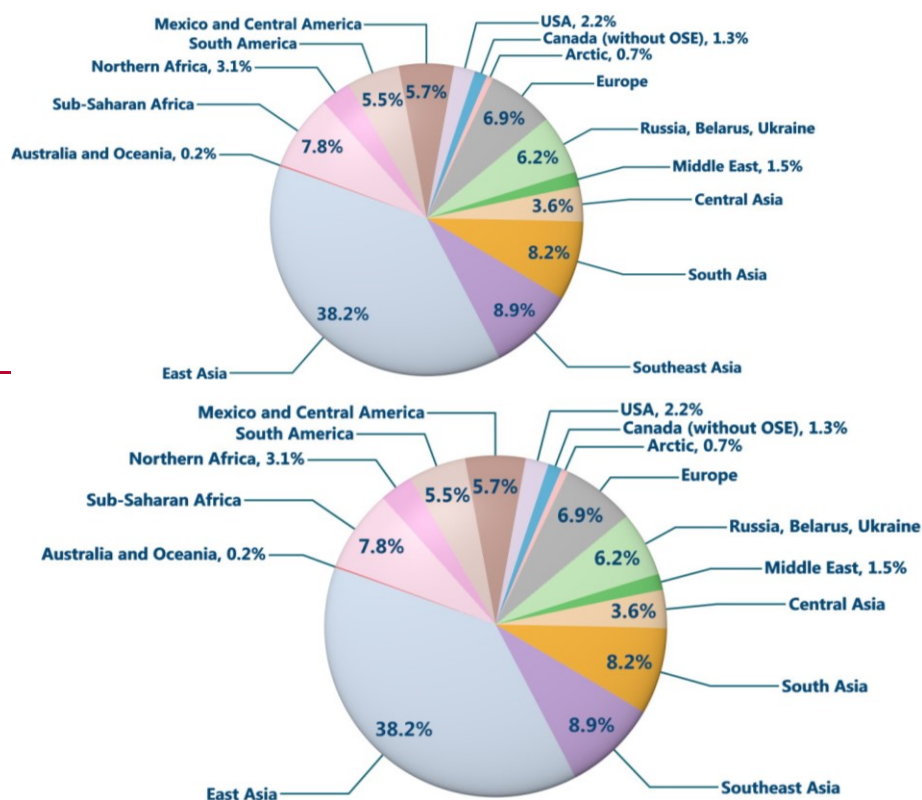
889

890 **Source apportionment of the background mercury deposition**

891 As noticed in Figure 14-16, background Hg (long-range transport from global source regions;  
 892 excludes impact of oil sands emissions, but includes impact of all other Hg emissions in Canada)  
 893 is responsible for the majority of annual Hg deposition in the AOSR (except in winter in the  
 894 vicinity of major oil sands Hg emission sources). The average annual background Hg deposition  
 895 in the AOSR was  $15.3\text{-}16.7 \mu\text{g m}^{-2}\text{y}^{-1}$  in 2012-2015. This includes  $\sim 40\%$  deposition from  
 896 contemporary global anthropogenic Hg emissions (excluding Hg emissions from Athabasca oils  
 897 sands activities) and  $\sim 60\%$  from global geogenic emissions and re-emissions of legacy mercury  
 898 deposition (of both anthropogenic and geogenic origin). The model was applied to investigate the  
 899 relative proportions of background anthropogenic Hg deposition fluxes contributed from various

900 worldwide emission source regions, including Canada, in the AOSR (Figure 18). Almost 50% of  
 901 the background anthropogenic Hg deposition originated from East and Southeast Asia, a region of  
 902 high economic activity and high energy demand, which is sourced for the most part by coal-fired  
 903 power plants. The model estimated that foreign anthropogenic sources accounted for over 98% of  
 904 the background anthropogenic Hg deposition in the AOSR of which present-day emissions in East  
 905 Asia, Southeast Asia, South Asia, Sub-Saharan Africa, Europe and the United States contributed  
 906 to approximately 38%, 9%, 8%, 8%, 7%, and 2%, respectively. Emissions from present-day  
 907 anthropogenic sources in Canada (excluding oil sands sources in AOSR) contributed to < 2% of  
 908 the background anthropogenic Hg deposition nationally including the AOSR. In proximity of oil  
 909 sands activities, oil sand Hg ~~emissions~~emissions are a significant source of Hg deposition as  
 910 demonstrated earlier in this study. By comparison, oil sands developments currently have a  
 911 negligible impact on Hg deposition on a broader spatial scale in Canada. These results highlight  
 912 the need for worldwide mitigation efforts, in addition to the local efforts, to reduce the risks of  
 913 mercury contamination in the AOSR.

914



915

916

917 Figure 18: Deposition contributions from global anthropogenic source regions (excluding  
918 Athabasca oil sands Hg emissions) to the average contemporary anthropogenic Hg deposition  
919 portion (40% of total deposition) of the total deposition in Athabasca Oil Sands Region in 2015.

920

## 921 **Conclusions**

922 An assessment of mercury levels in air and deposition in the Athabasca oil sands region (AOSR)  
923 in Northern Alberta, Canada, was conducted to investigate the contribution of Hg emitted from oil  
924 sands activities on the surrounding landscape using a 3D process-based Hg model in 2012-2015.

925 The model-simulated Hg burden in the region was first evaluated with multi-year observations of  
926 air concentrations of Hg and seasonally accumulated Hg in snow. Model-measurement agreement  
927 of Hg surface air concentrations and snow loadings in AOSR were within the measurement and  
928 modeling uncertainties and implies that NPRI reported emissions of Hg from oil sands operations  
929 (i.e., 59, 69, 44 and 25 kg in 2012, 2013, 2014 and 2015, respectively) are consistent with Hg  
930 burden in the region. Air concentrations of Hg(0) in the AOSR ( $1.4 \text{ ng m}^{-3}$ ) were at a similar level  
931 as found in Northern Alberta, and were within the range of concentrations in Canada ( $1.2\text{-}1.6 \text{ ng}$   
932  $\text{m}^{-3}$ ). Background Hg(0) concentrations in Canada are dominated by long-range transport, with a  
933 slightly larger impact in the west, and, thus, contribution of oil sands activities to Hg(0)  
934 concentrations in AOSR was minimal ( $< 0.1\%$ , average enrichment). During the summer season,  
935 Hg emissions originating from regional wildfires were found to be an episodically important  
936 source of atmospheric Hg(0), with daily averaged concentrations peaking to  $2.5 \text{ ng m}^{-3}$  (Parsons  
937 et al. 2013; Fraser et al., 2018). Average total oxidized Hg concentrations (gaseous plus  
938 particulate) in the air were elevated above background by 55% and 65% in 2012 and 2013,  
939 respectively, and over 10% in 2015 within 50 km of upgrading facilities (particularly in the  
940 northeast sector) in the AOSR as a result of oil sands emissions.

941

942 The level and spatial extent of the impact of oil sands emissions to winter, summer and annual Hg  
943 deposition fluxes were examined in high (2012-2013) and low (2014-2015) oil sands Hg emission  
944 years. In 2012-2015, annual average total Hg deposition fluxes of  $15.6\text{-}18.3 \text{ } \mu\text{g m}^{-2}\text{y}^{-1}$  were  
945 simulated in AOSR with deposition in winter (November-April) and summer (June-August)  
946 contributing to 20% and 50%, respectively. The emission sources of Hg deposition in the AOSR  
947 are global anthropogenic (including Canadian emissions), natural and reemissions of legacy Hg

948 deposition (including biomass burning emissions). Similar to other regions in Canada, on a broader  
949 scale, Hg deposition in the AOSR is dominated by mercury transported from global sources, with  
950 a small (and highly spatiotemporal variable) impact from regional biomass burning events. In  
951 proximity to oil sands sources, however, total Hg deposition in wintertime was largely driven by  
952 oil sands emissions. Deposition increases of up to 146-500% occurred within 10 km of oil sands  
953 sources in the high emission years 2012 and 2013; summertime and annual Hg deposition increases  
954 due to oil sands emissions were 13-56% and 24-70%, respectively, within 10 km of sources for  
955 the same years. In lower oil sands emission years (2014 and 2015), Hg deposition increases due to  
956 oil sands activities declined to 40-104% in winter and 5-14% annually within 10 km of oil sands  
957 sources. At 20 km from the oil sands operations, oil sands-related Hg deposition enhancements  
958 were not as large, with increases of 57-75% in winter, and 10% annually in 2012 and 2013. The  
959 spatial extent of the OSE influence on Hg deposition was also greater in winter relative to summer  
960 (~100 km vs 30 km from major Hg emitting facilities).

961  
962 Finally, factors contributing to the inter-annual variations (i.e., changes in meteorological  
963 conditions, oil sands emissions and wildfire emissions) in seasonal and annual Hg deposition  
964 fluxes and relative source attributions in AOSR were examined from 2012 to 2015. Wintertime  
965 (net) Hg deposition to northern landscapes is controlled by Hg deposition to snowpacks by direct  
966 uptake and via snowfall and post-depositional processes, which exhibit strong inter-annual  
967 variations. Relative to 2012, while changes in meteorological conditions led to a reduction in  
968 wintertime Hg net deposition fluxes by ~ 17% in 2013-2014, and an increase by 10% in 2015  
969 within 10 km of oil sands sources, changes in oil sands emissions led to deposition reductions of  
970 10%, 35% and 56% in 2013, 2014 and 2015, respectively, resulting in an overall reduction in  
971 wintertime Hg depositions of 27%, 52% and 46% in 2013, 2014 and 2015, respectively.  
972 Gopalapillai et al. (2019) reported temporal decline in snowpack total Hg loadings near-field, from  
973 an average load of 510 to 175 ng/m<sup>2</sup> from 2008 to 2016. At a distance of 10-20 km from the oil  
974 sands sources, while changes in meteorology led to a 54% increase in wintertime deposition in  
975 2015 relative to 2012, the decline in oil sands emissions led to a reduction in the deposition by  
976 35%, resulting in an overall increase in Hg deposition of 19%. Summertime Hg deposition to  
977 terrestrial systems is temporally less variable than wintertime deposition as it is predominantly  
978 driven by Hg uptake by vegetation and soils, and by wet deposition; thus, changes in oil sands

979 emissions played a more significant role in summertime inter-annual variations in Hg deposition  
980 than the meteorological factors. Compared to 2012, changes in meteorology, biomass burning and  
981 oil sand emissions led to changes in summertime deposition by -3%, -2%, and +7% in 2013, +3%,  
982 +2% and -15% in 2014, and -1%, +4% and -20% in 2015, resulting in overall changes in Hg  
983 deposition by +2%, -10% and -17% in 2013, 2014 and 2015, respectively, within 10 km of major  
984 oil sands sources. On an annual basis, in 2014 and 2015, variations in meteorology and biomass  
985 burning emissions led to deposition increases of 1-6% and 2%, respectively, and reduction in oil  
986 sands Hg emissions led to declines between 15-22%, resulting in an overall reduction in annual  
987 Hg deposition of 7-20% within 10 km of AR6. In 2015, at 10-20 km away from sources, Hg  
988 deposition increase due to changes in meteorology plus biomass burning was approximately equal  
989 to deposition decline due to changes in oil sands emissions, resulting in smaller (<8%) changes in  
990 Hg deposition fluxes.

991  
992 Oil sands Hg emissions are found to be important sources of Hg contamination to the local  
993 landscape in proximity of the processing activities, particularly in wintertime. Although Hg  
994 deposition is higher in summertime (mainly driven by long-range transport), oil sands Hg  
995 emissions contribute to a notably higher proportion of deposition in wintertime in the AOSR. Thus,  
996 the impact of oil sands emissions is more easily detected in snow Hg observations (Kirk et al.,  
997 2014). Wintertime Hg deposition rates are also more influenced by interannual changes in  
998 meteorological conditions compared to summer. Regarding the environmental importance of  
999 seasonal Hg deposition, it is likely that a major portion of summertime deposition remains bound  
1000 to vegetation and subsequently transferred to soils, where it can be partially sequestered and partly  
1001 reemitted back to air or mobilized in aquatic systems on long timescales of decades to centuries  
1002 (Zhou et al. 2021). In contrast, wintertime deposition (and partially summertime wet deposition)  
1003 can be transferred to the local aquatic system via runoff more readily (i.e, on an annual time scale).  
1004 Model findings reveal that year-to-year changes in meteorological conditions not only significantly  
1005 influence the rate of Hg deposition but, additionally, can either exacerbate or diminish the impact  
1006 of changes in oil sands emissions on Hg deposition, particularly in winter. Thus, meteorological  
1007 changes can confound the interpretation of trends in short-term monitoring data. In addition,  
1008 meteorological changes related to climate change can influence the deposition trends. Accurate  
1009 reporting of point and area Hg emissions related to oil sands activities, long-term monitoring of

1010 Hg in air and terrestrial ecosystems, and the application of process-based Hg models are crucial to  
1011 understanding systematic changes in Hg levels and their causes in the AOSR.

1012

### 1013 **Acknowledgements**

1014 We thank our ECCC colleagues Paul Makar, Sandro Leonardelli and Stewart Cober and in the  
1015 Pollutant Inventory and Reporting Division for their insightful comments and careful internal  
1016 review of the manuscript. This project was supported by the Joint Oil Sands Monitoring (JOSM)  
1017 program of ECCC.

1018

1019

### 1020 **References**

1021 Alexander, A. C. and Chambers, P. A.: Assessment of seven Canadian rivers in relation to stages  
1022 in oil sands industrial development, 1972–2010, *Environmental Reviews* 24, 484–494,  
1023 <https://doi.org/10.1139/er-2016-0033>, 2016.

1024 AMAP and UNEP: Technical Background Report for the Global Mercury Assessment 2013.  
1025 Chapter 3. Atmospheric Pathways, Transport and Fate., 263, 2013.

1026 Angot, H., Dastoor, A., De Simone, F., Gårdfeldt, K., Gencarelli, C. N., Hedgecock, I. M.,  
1027 Langer, S., Magand, O., Mastromonaco, M. N., Nordstrøm, C., Pfaffhuber, K. A., Pirrone,  
1028 N., Ryjkov, A., Selin, N. E., Skov, H., Song, S., Sprovieri, F., Steffen, A., Toyota, K.,  
1029 Travnikov, O., Yang, X., and Dommergue, A.: Chemical cycling and deposition of  
1030 atmospheric mercury in polar regions: review of recent measurements and comparison with  
1031 models, *Atmospheric Chemistry and Physics* 16, 10735–10763,  
1032 <https://doi.org/10.5194/acp-16-10735-2016>, 2016.

1033 APEI: Government of Canada, Air Pollutant Emissions Inventory,  
1034 [https://www.canada.ca/en/environment-climate-change/services/pollutants/air-emissions-](https://www.canada.ca/en/environment-climate-change/services/pollutants/air-emissions-inventory-overview.html)  
1035 [inventory-overview.html](https://www.canada.ca/en/environment-climate-change/services/pollutants/air-emissions-inventory-overview.html), accessed 25 Jul 2019

1036 Bieser, J., Slemr, F., Ambrose, J., Brenninkmeijer, C., Brooks, S., Dastoor, A., DeSimone, F.,  
1037 Ebinghaus, R., Gencarelli, C. N., Geyer, B., Gratz, L. E., Hedgecock, I. M., Jaffe, D.,  
1038 Kelley, P., Lin, C.-J., Jaegle, L., Matthias, V., Ryjkov, A., Selin, N. E., Song, S.,  
1039 Travnikov, O., Weigelt, A., Luke, W., Ren, X., Zahn, A., Yang, X., Zhu, Y., and Pirrone,  
1040 N.: Multi-model study of mercury dispersion in the atmosphere: vertical and



1041 interhemispheric distribution of mercury species, *Atmospheric Chemistry and Physics* 17,  
1042 6925–6955, <https://doi.org/10.5194/acp-17-6925-2017>, 2017.

1043 Bloom, N. S. and Crecelius, E. A.: Determination of mercury in seawater at sub-nanogram per  
1044 liter levels, *Marine chemistry* 14, 49–59, [https://doi.org/10.1016/0304-4203\(83\)90069-5](https://doi.org/10.1016/0304-4203(83)90069-5),  
1045 1983.

1046 CMSA: Canadian Mercury Science Assessment 2016, *Clean Air Regulatory Agenda*, 437–556,  
1047 2016.

1048 Cooke, C. A., Kirk, J. L., Muir, D. C. G., Wiklund, J. A., Wang, X., Gleason, A., and Evans, M.  
1049 S.: Spatial and temporal patterns in trace element deposition to lakes in the Athabasca oil  
1050 sands region (Alberta, Canada), *Environmental Research Letters* 12,  
1051 <https://doi.org/10.1088/1748-9326/aa9505>, 2017.

1052 Dastoor, A. P., Davignon, D., Theys, N., Van Roozendaal, M., Steffen, A., and Ariya, P. A.:  
1053 Modeling dynamic exchange of gaseous elemental mercury at polar sunrise, *Environmental*  
1054 *Science & Technology* 42, 5183–5188, 2008.

1055 Dastoor, A. P. and Durnford, D. A.: Arctic Ocean: Is it a sink or a source of atmospheric  
1056 mercury?, *Environmental Science & Technology* 48, 1707–1717,  
1057 <https://doi.org/10.1021/es404473e>, 2014.

1058 De Simone, F., Cinnirella, S., Gencarelli, C. N., Yang, X., Hedgecock, I. M., and Pirrone, N.:  
1059 Model study of global mercury deposition from biomass burning, *Environmental science &*  
1060 *technology* 49, 6712–6721, 2015.

1061 Durnford, D., Dastoor, A., Figueras-Nieto, D., and Ryjkov, A.: Long range transport of mercury  
1062 to the Arctic and across Canada, *Atmospheric Chemistry and Physics* 10, 6063–6086,  
1063 <https://doi.org/10.5194/acp-10-6063-2010>, 2010.

1064 Durnford, D., Dastoor, A., Ryzhkov, A., Poissant, L., Pilote, M., and Figueras-Nieto, D.: How  
1065 relevant is the deposition of mercury onto snowpacks?—Part 2: A modeling study,  
1066 *Atmospheric Chemistry and Physics* 12, 9251–9274, 2012.

1067 Eckley, C. S., Parsons, M. T., Mintz, R., Lapalme, M., Mazur, M., Tordon, R., Elleman, R.,  
1068 Graydon, J. A., Blanchard, P., and St Louis, V.: Impact of closing Canada’s largest point-  
1069 source of mercury emissions on local atmospheric mercury concentrations., *Environ Sci*  
1070 *Technol* 47, 10339–10348, <https://doi.org/10.1021/es401352n>, 2013.

1071 Emmerton, C. A., Cooke, C. A., Wentworth, G. R., Graydon, J. A., Ryjkov, A., and Dastoor, A.:  
1072 Total Mercury and Methylmercury in Lake Water of Canada's Oil Sands Region., Environ  
1073 Sci Technol 52, 10946–10955, <https://doi.org/10.1021/acs.est.8b01680>, 2018.

1074 EPA: United States Government: EPA Air Emissions Inventories, [https://www.epa.gov/air-](https://www.epa.gov/air-emissions-inventories)  
1075 [emissions-inventories](https://www.epa.gov/air-emissions-inventories); accessed 25 Jul 2019

1076 EPA: Method 1669: Sampling ambient water for trace metals at EPA water quality criteria  
1077 levels, 1996.

1078 Faïn, X., Helmig, D., Hueber, J., Obrist, D., and Williams, M. W.: Mercury dynamics in the  
1079 Rocky Mountain, Colorado, snowpack, Biogeosciences 10, 3793–3807, 2013.

1080 Fraser, A., Dastoor, A., and Ryjkov, A.: How important is biomass burning in Canada to  
1081 mercury contamination, Atmospheric Chemistry and Physics 18, 7263,  
1082 <https://doi.org/10.5194/acp-18-7263-2018>, 2018.

1083 Friedli, H. R., Radke, L. F., and Lu, J. Y.: Mercury in smoke from biomass fires, Geophysical  
1084 Research Letters 28, 3223–3226, 2001.

1085 GoC: Government of Canada, Historical Climate Data, <https://climate.weather.gc.ca>, accessed 19  
1086 Feb 2019

1087 Gopalapillai, Y., Kirk, J. L., Landis, M. S., Muir, D. C. G., Cooke, C. A., Gleason, A., Ho, A.,  
1088 Kelly, E., Schindler, D., Wang, X., and Lawson, G.: Source Analysis of Pollutant Elements  
1089 in Winter Air Deposition in the Athabasca Oil Sands Region: A Temporal and Spatial  
1090 Study, ACS Earth and Space Chemistry 3, 1656–1668,  
1091 <https://doi.org/10.1021/acsearthspacechem.9b00150>, 2019.

1092 Graydon, J. A., St. Louis, V. L., Lindberg, S. E., Hintelmann, H., and Krabbenhoft, D. P.:  
1093 Investigation of Mercury Exchange between Forest Canopy Vegetation and the  
1094 Atmosphere Using a New Dynamic Chamber, Environmental Science & Technology  
1095 40, 4680–4688, <https://doi.org/10.1021/es0604616>, 2006.

1096 Gustin, M. S., Huang, J., Miller, M. B., Peterson, C., Jaffe, D. A., Ambrose, J., Finley, B. D.,  
1097 Lyman, S. N., Call, K., Talbot, R., Feddersen, D., Mao, H., and Lindberg, S. E.: Do We  
1098 Understand What the Mercury Speciation Instruments Are Actually Measuring? Results of  
1099 RAMIX., Environmental Science & Technology <https://doi.org/10.1021/es3039104>,  
1100 2013.

1101 Gustin, M. S., Amos, H. M., Huang, J., Miller, M. B., and Heidecorn, K.: Measuring and  
1102 modeling mercury in the atmosphere: a critical review, *Atmos. Chem. Phys.*, 15, 5697–  
1103 5713, <https://doi.org/10.5194/acp-15-5697-2015>, 2015.

1104 Jia, L.: Oil Sands Bitumen Emulsion Upgrading by Using In Situ Hydrogen Generated through  
1105 the Water Gas Shift Reaction, 2014.

1106 Kelly, E. N., Schindler, D. W., Hodson, P. V., Short, J. W., Radmanovich, R., and Nielsen, C.  
1107 C.: Oil sands development contributes elements toxic at low concentrations to the  
1108 Athabasca River and its tributaries, *Proceedings of the National Academy of Sciences* 107,  
1109 16178–16183, <https://doi.org/10.1073/pnas.1008754107>, 2010.

1110 Kirk, J. L., Muir, D. C. G., Gleason, A., Wang, X., Lawson, G., Frank, R. A., Lehnherr, I., and  
1111 Wrona, F.: Atmospheric deposition of mercury and methylmercury to landscapes and  
1112 waterbodies of the Athabasca oil sands region, *Environmental science & technology* 48,  
1113 7374–7383, 2014.

1114 Kos, G., Ryzhkov, A., Dastoor, A., Narayan, J., Steffen, A., Ariya, P. A., and Zhang, L.:  
1115 Evaluation of discrepancy between measured and modelled oxidized mercury species,  
1116 *Atmospheric Chemistry and Physics* 13, 4839–4863, [https://doi.org/10.5194/acp-13-4839-](https://doi.org/10.5194/acp-13-4839-2013)  
1117 2013, 2013.

1118 Larter, S. R. and Head, I. M.: Oil sands and heavy oil: origin and exploitation, *Elements* 10, 277–  
1119 283, 2014.

1120 Lynam, M., Dvonch, J. T., Barres, J., and Percy, K.: Atmospheric wet deposition of mercury to  
1121 the Athabasca oil sands region, Alberta, Canada, *Air Quality, Atmosphere & Health* 11,  
1122 83–93, 2018.

1123 Ma, J., Hintelmann, H., Kirk, J., and Muir, D.: Mercury concentrations and mercury isotope  
1124 composition in lake sediment cores from the vicinity of a metal smelting facility in Flin  
1125 Flon, Manitoba, *Chemical Geology* <https://doi.org/10.1016/j.chemgeo.2012.10.037>, 2012.

1126 Makar, P., Akingunola, A., Pabla, B., Stroud, C., Chen, J., Cheung, P., Moran, M., Gong, W.,  
1127 Zheng, Q., and Li, S. M.: Experimental Forecasting Using the High-Resolution Research  
1128 Configuration of GEM-MACH, *International Technical Meeting on Air Pollution*  
1129 *Modelling and its Application*, 225–230, 2018.

1130 Muir, D.C.G., Wang, X., Yang, F., Nguyen, N., Jackson, T.A., Evans, M.S., Douglas, M., Kock, G.,  
1131 Lamoureux, S., Pienitz, R., Smol, J.P., Vincent, W.F., Dastoor, A. (2009). ‘Spatial trends and historical

1132 deposition of mercury in eastern and northern Canada inferred from lake sediment cores.’ Environment  
1133 Science & Technology, 43, 4802 – 4809.

1134

1135 NPRI: Government of Canada, Access the reporting guide for the National Pollutant Release  
1136 Inventory, [https://www.canada.ca/en/environment-climate-change/services/national-](https://www.canada.ca/en/environment-climate-change/services/national-pollutant-release-inventory/report/access-reporting-guide.html)  
1137 [pollutant-release-inventory/report/access-reporting-guide.html](https://www.canada.ca/en/environment-climate-change/services/national-pollutant-release-inventory/report/access-reporting-guide.html), accessed 25 Jul 2019

1138 NPRI: Government of Canada, National Pollutant Release Inventory, [https://www.ec.gc.ca/inrp-](https://www.ec.gc.ca/inrp-npri/)  
1139 [npri/](https://www.ec.gc.ca/inrp-npri/), accessed 25 Jul 2019

1140 Obrist, D., Johnson, D. W., and Edmonds, R. L.: Effects of vegetation type on mercury  
1141 concentrations and pools in two adjacent coniferous and deciduous forests, *Journal of Plant*  
1142 *Nutrition and Soil Science* 175, 68–77, <https://doi.org/10.1002/jpln.201000415>, 2012.

1143 Obrist, D. *et al.* A synthesis of terrestrial mercury in the western United States: Spatial  
1144 distribution defined by land cover and plant productivity. *Science of the Total Environment*  
1145 568, 522-535, doi:10.1016/j.scitotenv.2015.11.104 (2016).

1146 Parsons, M., McLennan, D., Lapalme, M., Mooney, C., Watt, C., and Mintz, R.: Total gaseous  
1147 mercury concentration measurements at Fort McMurray, Alberta, Canada, *Atmosphere* 4,  
1148 472–493, <https://doi.org/10.3390/atmos4040472>, 2013.

1149 Steffen, A. and Schroeder, W. H.: Standard Operating Procedures Manual Procedure for Total  
1150 Gaseous Mercury Measurements-Canadian Atmospheric Mercury Measurement Network  
1151 (CAMNet), Meteorological Service of Canada 4905, 1999.

1152 Travnikov, O., Angot, H., Artaxo, P., Bencardino, M., Bieser, J., D’Amore, F.,  
1153 Dastoor, A., De Simone, F., Diéguez, M. D. C., Dommergue, A., Ebinghaus, R., Feng, X.  
1154 B., Gencarelli, C. N., Hedgecock, I. M., Magand, O., Martin, L., Matthias, V., Mashyanov,  
1155 N., Pirrone, N., Ramachandran, R., Read, K. A., Ryjkov, A., Selin, N. E., Sena, F., Song,  
1156 S., Sprovieri, F., Wip, D., Wängberg, I., and Yang, X.: Multi-model study of mercury  
1157 dispersion in the atmosphere: atmospheric processes and model evaluation, *Atmospheric*  
1158 *Chemistry and Physics* 17, 5271–5295, <https://doi.org/10.5194/acp-17-5271-2017>, 2017.

1159 UN: Minamata Convention on Mercury, 72, 2017, <http://www.mercuryconvention.org>.

1160 UNEP: The Global Atmospheric Mercury Assessment: Sources, Emissions and Transport, 2008.

1161 UNEP: Global Mercury Assessment 2013, Sources, Emissions, Releases and Environmental  
1162 Transport, 2013.

1163 UNEP: Global Mercury Assessment 2018, 2018.

1164 Wasiuta, V., Kirk, J. L., Chambers, P. A., Alexander, A. C., Wyatt, F. R., Rooney, R. C., and  
1165 Cooke, C. A.: Accumulating Mercury and Methylmercury Burdens in Watersheds  
1166 Impacted by Oil Sands Pollution., *Environ Sci Technol* 53, 12856–12864,  
1167 <https://doi.org/10.1021/acs.est.9b02373>, 2019.

1168 Whaley, C. H., Galarneau, E., Makar, P. A., Akingunola, A., Gong, W., Gravel, S., Moran, M.  
1169 D., Stroud, C., Zhang, J., and Zheng, Q.: GEM-MACH-PAH (rev2488): a new high-  
1170 resolution chemical transport model for North American polycyclic aromatic hydrocarbons  
1171 and benzene, *Geoscientific Model Development* 11, 2609–2632,  
1172 <https://doi.org/10.5194/gmd-11-2609-2018>, 2018.

1173 Wiedinmyer, C., Akagi, S. K., Yokelson, R. J., Emmons, L. K., Al-Saadi, J. A., Orlando, J. J.,  
1174 and Soja, A. J.: The Fire INventory from NCAR (FINN): A high resolution global model to  
1175 estimate the emissions from open burning, *Geoscientific Model Development* 4, 625, 2011.

1176 Wiedinmyer, C. and Friedli, H.: Mercury emission estimates from fires: An initial inventory for  
1177 the United States, *Environmental science & technology* 41, 8092–8098,  
1178 <https://doi.org/10.1021/es071289o>, 2007.

1179 Willis, C. E., Kirk, J. L., St Louis, V. L., Lehnerr, I., Ariya, P. A., and Rangel-Alvarado, R. B.:  
1180 Sources of Methylmercury to Snowpacks of the Alberta Oil Sands Region: A Study of In  
1181 Situ Methylation and Particulates., *Environ Sci Technol* 52, 531–540,  
1182 <https://doi.org/10.1021/acs.est.7b04096>, 2018.

1183 Willis, C. E., St Louis, V. L., Kirk, J. L., St Pierre, K. A., and Dodge, C.: Tailings ponds of the  
1184 Athabasca Oil Sands Region, Alberta, Canada, are likely not significant sources of total  
1185 mercury and methylmercury to nearby ground and surface waters., *Sci Total Environ* 647,  
1186 1604–1610, <https://doi.org/10.1016/j.scitotenv.2018.08.083>, 2019.

1187 Wright, L. P., Zhang, L., and Marsik, F. J.: Overview of mercury dry deposition, litterfall, and  
1188 throughfall studies, *Atmospheric Chemistry and Physics* 16, 13399,  
1189 <https://doi.org/10.5194/acp-16-13399-2016>, 2016.

1190 Zhang, L., Wright, L. P. & Blanchard, P. A review of current knowledge concerning dry  
1191 deposition of atmospheric mercury. *Atmospheric Environment* 43, 5853-5864, 2009.

1192 Zhang, J., Moran, M. D., Zheng, Q., Makar, P. A., Baratzadeh, P., Marson, G., Liu, P., and Li,  
1193 S.-M.: Emissions preparation and analysis for multiscale air quality modeling over the

1194 Athabasca Oil Sands Region of Alberta, Canada, *Atmospheric Chemistry and Physics* 18,  
1195 10459–10481, 2018.

1196 Zhang, L., Wu, Z., Cheng, I., Wright, L. P., Olson, M. L., Gay, D. A., Risch, M. R., Brooks, S.,  
1197 Castro, M. S., Conley, G. D., Edgerton, E. S., Holsen, T. M., Luke, W., Tordon, R., and  
1198 Weiss-Penzias, P.: The estimated six-year mercury dry deposition across North America,  
1199 *Environ. Sci. Technol.*, 50, 12864–12873, <https://doi.org/10.1021/acs.est.6b04276>, 2016.

1200 Zhou, J., Obrist, D., Dastoor, A., Jiskra, M., and Ryjkov, A.: Vegetation uptake of mercury and  
1201 impacts on global cycling, *Nature Reviews Earth & Environment*, 1-16,  
1202 [https://doi.org/10.1038/s43017-021-00146-](https://doi.org/10.1038/s43017-021-00146-y) y, 2021.

1203